Cell Reports

Article

Maternal γδ T cells shape offspring pulmonary type 2 immunity in a microbiota-dependent manner

Graphical abstract

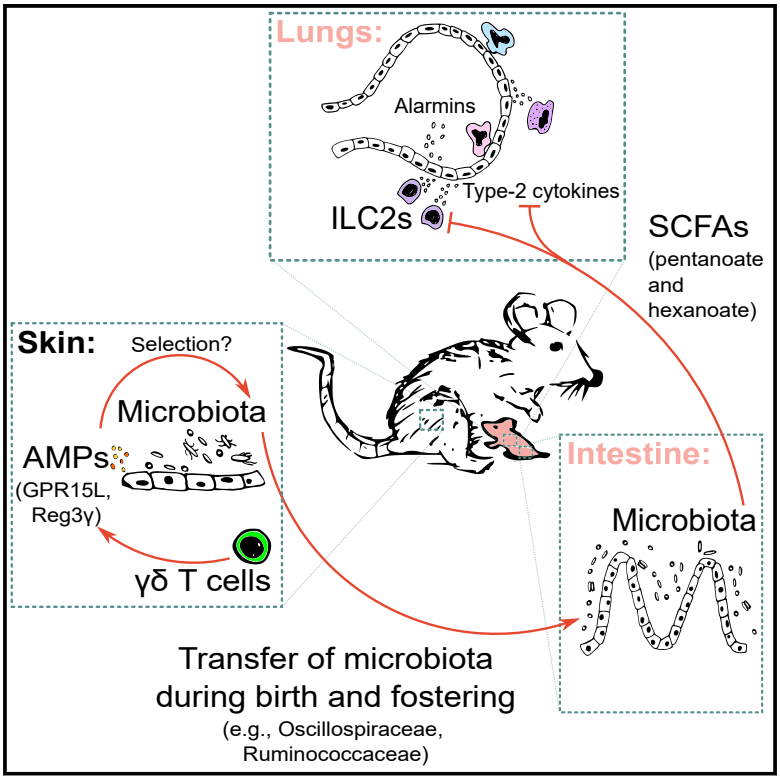

Highlights

- The offspring of γδ T cell-deficient dams display enhanced lung type 2 immunity
- *TCRδ*$^{-/-}$ dams display differences in AMP levels and microbiota composition in the skin
- Transfer of microbiota during birth and fostering regulates the first-breath reaction
- SCFAs pentanoate and hexanoate suppress ILC2 functions and lung inflammation

Authors

Pedro H. Papotto, Bahtiyar Yilmaz, Gonçalo Pimenta, ..., Andrew J. Macpherson, Judith E. Allen, Bruno Silva-Santos

Correspondence

pedro.papotto@manchester.ac.uk (P.H.P.), bssantos@medicina.ulisboa.pt (B.S.-S.)

In brief

Papotto et al. show that the offspring of γδ T cell-deficient dams acquire perinatally a gut microbiota with decreased capacity of short-chain fatty acid (SCFA) production, leading to enhanced lung type 2 immune activation during steady state and infection. This regulatory neonatal gut-lung axis acts via the SCFAs pentanoate and hexanoate.

Papotto et al., 2023, Cell Reports *42*, 112074
February 28, 2023
https://doi.org/10.1016/j.celrep.2023.112074

CellPress

Cell Reports

CellPress
OPEN ACCESS

Article

Maternal γδ T cells shape offspring pulmonary type 2 immunity in a microbiota-dependent manner

Pedro H. Papotto,[1,2,*] Bahtiyar Yilmaz,[3,4,6] Gonçalo Pimenta,[1,6] Sofia Mensurado,[1] Carolina Cunha,[1] Gina J. Fiala,[1] Daniel Gomes da Costa,[1] Natacha Gonçalves-Sousa,[1] Brian H.K. Chan,[2,5] Birte Blankenhaus,[1] Rita G. Domingues,[2] Tânia Carvalho,[1] Matthew R. Hepworth,[2] Andrew J. Macpherson,[3,4] Judith E. Allen,[2,5] and Bruno Silva-Santos[1,7,*]

[1]Instituto de Medicina Molecular João Lobo Antunes, Faculdade de Medicina, Universidade de Lisboa, Lisbon, Portugal
[2]Lydia Becker Institute for Immunology & Infection, Faculty of Biology, Medicine & Health, Manchester Academic Health Science Centre, University of Manchester, Manchester, UK
[3]Maurice Müller Laboratories, Department for Biomedical Research, University of Bern, Bern, Switzerland
[4]Department of Visceral Surgery and Medicine, Bern University Hospital, University of Bern, Bern, Switzerland
[5]Wellcome Centre for Cell-Matrix Research, Faculty of Biology, Medicine & Health, Manchester Academic Health Science Centre, University of Manchester, Manchester, UK
[6]These authors contributed equally
[7]Lead contact
*Correspondence: pedro.papotto@manchester.ac.uk (P.H.P.), bssantos@medicina.ulisboa.pt (B.S.-S.)
https://doi.org/10.1016/j.celrep.2023.112074

SUMMARY

Immune development is profoundly influenced by vertically transferred cues. However, little is known about how maternal innate-like lymphocytes regulate offspring immunity. Here, we show that mice born from γδ T cell-deficient (*TCRδ*$^{-/-}$) dams display an increase in first-breath-induced inflammation, with a pulmonary milieu selectively enriched in type 2 cytokines and type 2-polarized immune cells, when compared with the progeny of γδ T cell-sufficient dams. Upon helminth infection, mice born from *TCRδ*$^{-/-}$ dams sustain an increased type 2 inflammatory response. This is independent of the genotype of the pups. Instead, the offspring of *TCRδ*$^{-/-}$ dams harbors a distinct intestinal microbiota, acquired during birth and fostering, and decreased levels of intestinal short-chain fatty acids (SCFAs), such as pentanoate and hexanoate. Importantly, exogenous SCFA supplementation inhibits type 2 innate lymphoid cell function and suppresses first-breath- and infection-induced inflammation. Taken together, our findings unravel a maternal γδ T cell-microbiota-SCFA axis regulating neonatal lung immunity.

INTRODUCTION

The development of the immune system is particularly sensitive to maternally derived factors.[1] Maternal transfer of bacterial species during pregnancy and pre-weaning is responsible for determining the offspring's microbiota profile, which in turn influences immune responses later in life.[2–4] For example, vertical transfer of bacterial products via antibodies during pregnancy was shown to modulate the maturation of the intestinal immune system in the offspring.[5] Maternally transferred antibodies were also recently shown to control the homeostatic number of colonic regulatory T (T_{reg}) cells across generations.[6] Furthermore, maternal exposure to a high-fiber diet during pregnancy leads to decreased airway allergic disease severity in their progeny through the transfer of short-chain fatty acids (SCFAs), a major class of dietary metabolites.[7] Interestingly, airway immune disorders seem to be tightly connected with early-life exposure to environmental challenges,[8] likely due to type 2 immune activation and tissue remodeling characterizing the perinatal phase of lung development.[9,10] Apart from exciting biological consequences, this maternal cross-talk has profound implications on the design of experiments using genetically engineered mice, namely the choice of controls to generate accurate and reproducible data. Even though littermate controls are considered the gold standard,[11] it is clear that alternative approaches, such as co-housing and especially genetic background matching (to so-called "wild-type" mice, often obtained directly from commercial vendors), are still widely used in biomedical research. However, given that many external cues are vertically transferred during early life and have long-lasting consequences,[5–7,12] controlling for environmental factors without using littermate controls is nearly impossible. On a positive note, the problems evidenced by the use of suboptimal controls raise interesting questions on how parental-derived factors affect the offspring.[13,14] In particular, even though the maternal influence on progeny immune system is evident, the role of individual components of the maternal immune system (beyond antibodies) in regulating the immune status of the offspring remains largely unexplored.

γδ T cells are a population of innate-like lymphocytes known to reside in different tissues that compose the maternal-newborn

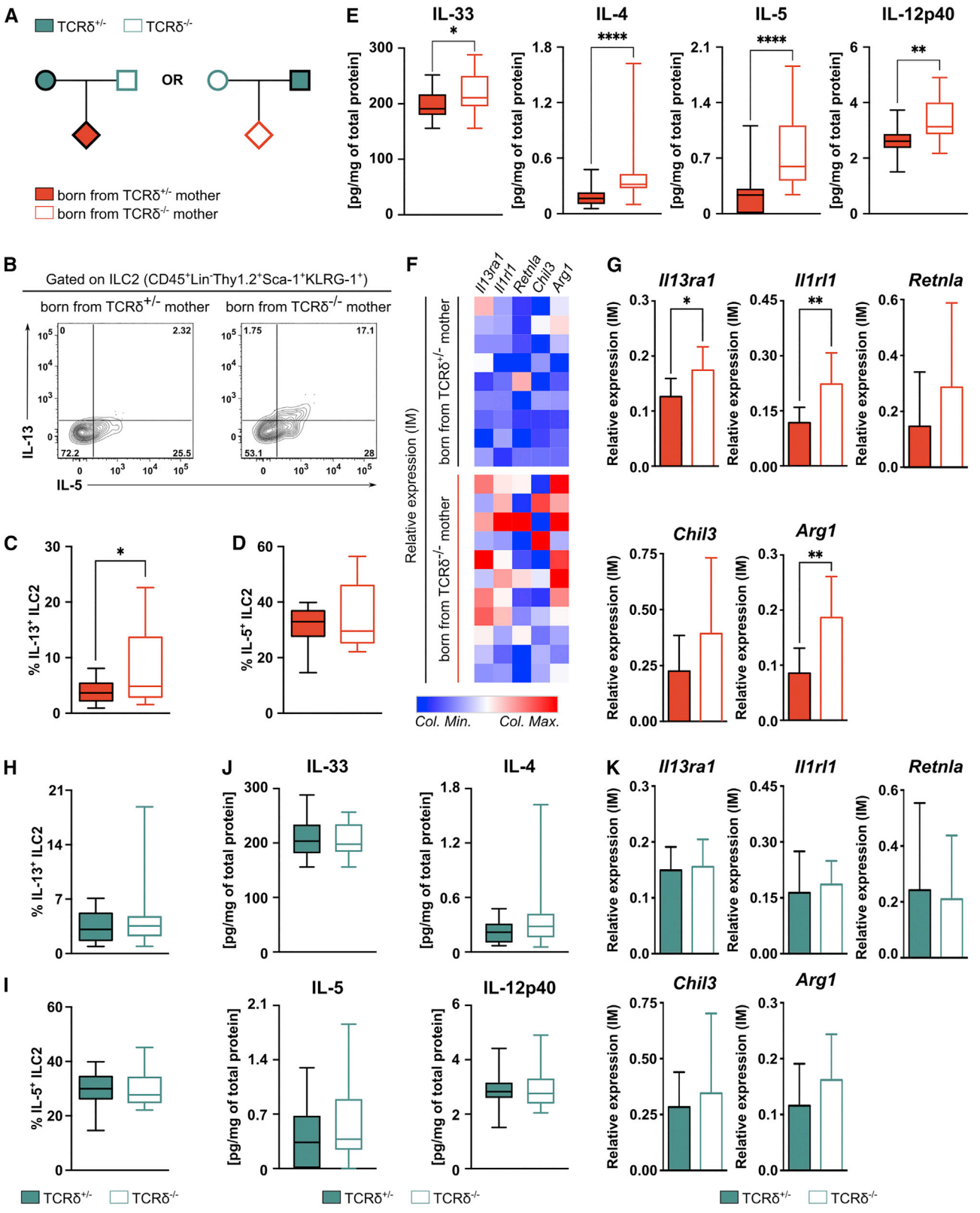

(legend on next page)

interface, such as the female reproductive tract,[15–17] the skin,[18,19] and mammary gland.[20] Murine γδ T cells were shown to control antibody production both under steady-state conditions[21] and upon challenge.[22] Also, γδ T cells are known to participate in an intricate cross-talk with barrier tissue microbiota,[23,24] notably being able to exert significant selective pressure on bacterial communities, as recently documented for the oral microbiome.[25,26] Hence, we aimed to determine if and how maternal γδ T cells affect offspring immune system development. Here, we show that pups born from *TCRδ*$^{-/-}$ (compared with *TCRδ*$^{+/-}$) dams present a perinatal pulmonary environment strongly biased toward type 2 immunity, both in the steady state and upon helminth infection, irrespective of their own genotype. Based on cross-fostering and cesarean section (C-Sec) delivery experiments, as well as antibiotic treatment and metabolomic approaches, we propose a critical role for the microbiota and their metabolic byproducts in this process.

RESULTS

Absence of maternal γδ T cells exacerbates perinatal pulmonary type-2 immune activation in offspring

The importance of pulmonary γδ T cells in the establishment of lung type 2 immune responses has been highlighted by various groups.[27–29] While trying to understand the mechanisms underlying the γδ T cell-type 2 immunity cross-talk, we observed that mice from our *TCRδ*$^{-/-}$ colony (*TCRδ*$^{-/-}$ × *TCRδ*$^{-/-}$) possessed decreased frequencies and numbers of pulmonary type 2 innate lymphoid cells (ILC2s) when compared with age- and sex-matched adult C57BL6/J mice (Figures S1A and S1B). However, and intriguingly, when we compared *TCRδ*$^{+/+}$ and *TCRδ*$^{-/-}$ littermates from heterozygous breedings (*TCRδ*$^{+/-}$ × *TCRδ*$^{+/-}$), no differences were observed in lung ILC2s, suggesting that this was not dependent on offspring genotype (Figure S1C and S1D). Moreover, when infected with the helminth *Nippostrongylus brasiliensis*, a parasite that induces a damage/repair cycle in the lungs that is highly dependent on type 2 immunity,[30] *TCRδ*$^{-/-}$ mice presented increased lung damage compared with C57BL6/J mice (Figures S1E and S1F). However, *TCRδ*$^{-/-}$ and *TCRδ*$^{+/+}$ littermates showed comparable lung damage upon infection (Figures S1G and S1H). As our *TCRδ*$^{+/-}$ breeding is derived from the *TCRδ*$^{-/-}$ colony, and both experience the same environmental factors, we hypothesized that the absence of γδ T cells in the dams could be responsible for altered lung ILC2s. To test this hypothesis, we established reciprocal breeding colonies by crossing *TCRδ*$^{-/-}$ females with *TCRδ*$^{+/-}$ males, and vice versa; these breeding strategies give rise to both *TCRδ*$^{-/-}$ and *TCRδ*$^{+/-}$ progeny, allowing us to exclude gene-intrinsic effects in the offspring (Figure 1A). We chose to analyze the lungs of pups born from γδ-deficient and -sufficient dams around postnatal day (PN) 15, as the main events leading to the maturation of the pulmonary immune system peak during this time as a consequence of the first-breath-induced inflammatory reaction.[9,10] In accordance with our hypothesis, pups born from *TCRδ*$^{-/-}$ dams exhibited a decrease in lung ILC2s when compared with pups born from *TCRδ*$^{+/-}$ dams (Figures S1J and S1K). Interestingly, the offspring of *TCRδ*$^{-/-}$ dams displayed augmented perinatal pulmonary type 2 activation, including increases in interleukin-13 (IL-13)$^{+}$, but not IL-5^{+}, ILC2s (Figures 1B–1D) and IL-5^{+} mast cells (Figures S1N–S1P). Accordingly, we also observed increased tissue levels of the type 2-inducing alarmin IL-33, and the type 2 cytokines IL-4 and IL-5, in the lungs of the progeny of *TCRδ*$^{-/-}$ dams when compared with pups born from their *TCRδ*$^{+/-}$ counterparts (Figure 1E). In addition, consistent with findings in type 2 asthma models,[31] IL-12p40, but not IL-12p70 and IL-23, was also increased in the lungs of the offspring from *TCRδ*$^{-/-}$ dams (Figures 1E and S1S). Moreover, interstitial macrophages from the offspring of *TCRδ*$^{-/-}$ dams exhibited a significant, albeit small, increase in the expression of type 2-regulated genes, such as *Il13ra*, *Il1rl1*, and *Arg1* (Figures 1F and 1G). Critically, when the same pups were stratified according to their own genotype, no differences were observed between *TCRδ*$^{-/-}$ and *TCRδ*$^{+/-}$ pups regarding lung ILC2s (Figures 1H, 1I, S1L, and S1M), mast cells (Figures S1Q and S1R), lung cytokine levels (Figure 1J), or gene expression on interstitial macrophages (Figure 1K). Thus, the observed increase in first-breath-induced type 2 immune responses in pups born from *TCRδ*$^{-/-}$ dams depends solely on the maternal genotype.

Of note, despite the differences observed in pulmonary type 2 immunity, pups born from *TCRδ*$^{-/-}$ and *TCRδ*$^{+/-}$ dams presented a similar distribution of lung myeloid populations (Figure S2A), T and B lymphocytes (Figure S2B), and T_{reg} cells (Figure S2C). Moreover, the expression of epithelial genes

Figure 1. Absence of maternal γδ T cells exacerbates first-breath-induced type 2 inflammation in the offspring

(A) Breeding strategy employed to evaluate the gene-extrinsic and -intrinsic roles of γδ T cell depletion on the formation of the neonatal pulmonary immune system.

(B) Flow cytometry analysis of intracellular IL-5 and IL-13 in ILC2s isolated from the lungs of pups described in (A) and stimulated *in vitro* for 3 h in the presence of PMA, ionomycin, and brefeldin A.

(C and D) Frequencies of (C) IL-13^{+} and (D) IL-5^{+} cells within the ILC2 population in the lungs.

(E) Concentration of cytokines within the whole lung homogenate normalized by total protein.

(F and G) Heatmap (F) and bar plots (G) depicting mRNA expression (relative to *Hprt* and *Actb*) of selected genes by qPCR in sorted interstitial macrophages (IMs) from the pups described in (A), grouped by maternal genotype.

(H and I) Frequencies of (H) IL-13^{+} and (I) IL-5^{+} cells within the ILC2 population in the lungs of pups depicted in (A), grouped by offspring genotype.

(J) Concentration of cytokines within the whole lung homogenate normalized by total protein.

(K) mRNA expression of selected genes by qPCR in sorted IMs, grouped by offspring genotype.

Data pooled from at least three independent litters per genotype. (B–D, H, and I) n = 16–17 mice per group.

(E–J) n = 18–23 mice per group. (G and K) n = 9–11 mice per group. (C–E and H–J) Box-and-whisker plots display first and third quartiles and the median; whiskers are from each quartile to the minimum or maximum. (G and K) Error bars represent mean ± SD. Normality of the samples was assessed with D'Agostino Pearson normality test; statistical analysis was then performed using Student's t test or Mann-Whitney test. *p < 0.05; **p < 0.01; ****p < 0.0001.

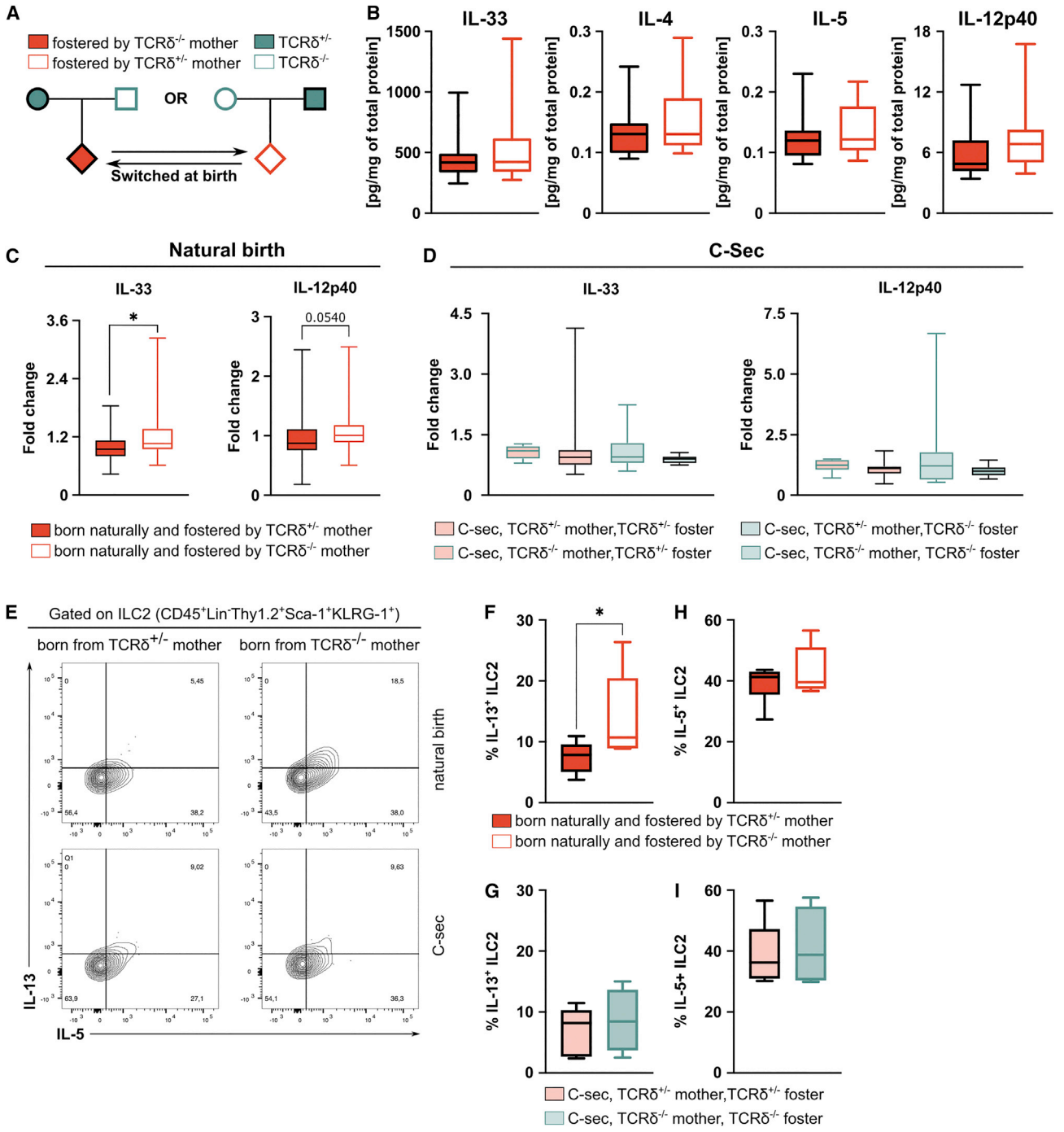

Figure 2. Maternal regulation of first-breath-induced inflammation in the offspring occurs during delivery and fostering

(A) Breeding strategy employed to evaluate the role of fostering on perinatal lung inflammation.

(B) Concentration of cytokines within the whole lung homogenate; concentration was normalized to the total protein in the tissue.

(C and D) Concentration of cytokines within the whole lung homogenate of pups born naturally or via C-Sec from *TCRδ*$^{+/-}$ or *TCRδ*$^{-/-}$ dams grouped by maternal and foster genotype; concentration was normalized to the fold change relative to pups born naturally from *TCRδ*$^{+/-}$ dams.

(E) Flow cytometry analysis of intracellular IL-5 and IL-13 in ILC2s isolated from the lungs and stimulated *in vitro* for 3 h in the presence of PMA, ionomycin, and brefeldin A.

(F–I) Frequencies of (F and G) IL-13^{+} and (H and I) IL-5^{+} cells within the ILC2 population in the lungs, grouped by maternal genotype and mode of delivery.

(legend continued on next page)

controlling surfactant and mucin production and barrier integrity was similar between pups from both breeding strategies (Figure S2D). Finally, the differences between the progeny of $TCR\delta^{-/-}$ and $TCR\delta^{+/-}$ dams seemed restricted to the lung, as we found similar frequencies of ILC2 precursors and other lymphoid and myeloid progenitors in the bone marrow (Figure S3A) and of innate lymphoid cells in the small intestine lamina propria (Figure S3B). These data indicate that maternal γδ T cells "vertically" (and selectively) regulate first-breath-induced pulmonary reaction in the offspring.

Microbiota transfer in early life mediates differences in the pulmonary immune system of the offspring from $TCR\delta^{+/-}$ and $TCR\delta^{-/-}$ dams

Transfer of maternally derived factors during pregnancy has been shown to regulate the development of the intestinal immune system[5,6] and suppress airway inflammation in the offspring.[7] Surprisingly, cross-fostering pups born from $TCR\delta^{-/-}$ dams with $TCR\delta^{+/-}$ surrogates, and vice versa (Figure 2A), abrogated the differences observed in the pulmonary milieu between their respective progeny (Figure 2B compared with Figure 1E). This suggested that the vertical conditioning of offspring lung immunity did not take place exclusively during pregnancy. To further rule out a role for maternally transferred factors during gestation and delivery, pups born via C-Sec from either $TCR\delta^{-/-}$ or $TCR\delta^{+/-}$ dams were co-fostered with pups naturally born (NB) by either a mother of the same or the opposite genotype (Figures 2C and 2D). Consistently, whereas NB pups from $TCR\delta^{-/-}$ dams retained increased lung levels of IL-33 and IL-13-producing pulmonary ILC2s, C-Sec delivery disrupted the increase in perinatal type 2 activation in the lungs of pups from $TCR\delta^{-/-}$ dams, irrespective of the foster mother (Figures 2D–2I). Of note, fostering pups born via C-Sec from $TCR\delta^{+/-}$ dams on their $TCR\delta^{-/-}$ counterparts did not induce an increase in lung inflammation (Figure 2D).

Maternal antibodies have been shown to prevent the development of asthma in the offspring through the control of aberrant type 2 immune responses,[32] and γδ T cells can regulate natural and adaptive antibody production.[21,22] However, the circulating levels of total immunoglobulin G (IgG) and IgG subclasses were similar between both $TCR\delta^{-/-}$ and $TCR\delta^{+/-}$ dams (Figures 3A and 3B) and their respective progeny (Figures 3A and 3C). Furthermore, we established reciprocal breeding colonies by crossing antibody-deficient JHT females with antibody-sufficient males, and vice versa (Figure 3D). As expected, the offspring of both JHT dams and their wild-type (WT) counterparts presented similar tissue levels of type 2 cytokines IL-33, IL-4, and IL-5 in their lungs and a slight increase in IL-12p40 (Figure 3E).

Vertical transfer of microbiota[4] or its products[5] has also been implicated in modulating offspring immunity. Hence, we treated parents and progeny from our reciprocal breeding strategies with a wide-spectrum antibiotic (ABX) cocktail starting from before pregnancy through gestation and fostering (Figure 3F). In contrast with the control setting (Figure 1E), pups born from ABX-treated $TCR\delta^{-/-}$ and $TCR\delta^{+/-}$ dams presented similar tissue levels of cytokines in their lungs (Figure 3G), suggesting that the enhanced type 2 pulmonary responses observed in pups born to $TCR\delta^{-/-}$ dams resulted from vertical transfer of microbiota or microbial-derived molecules.

$TCR\delta^{-/-}$ dams co-housed with $TCR\delta^{+/-}$ males retain differences in cutaneous bacterial communities

Co-housing is known to highly homogenizes the microbiota between different mouse colonies.[33] Thus, for our breeding setup, we expected to observe no differences in the microbiota of $TCR\delta^{-/-}$ and $TCR\delta^{+/-}$ dams upon co-housing with a male from the opposing genotype. In fact, before establishment of the reciprocal breeding pairs, $TCR\delta^{-/-}$ and $TCR\delta^{+/-}$ females displayed significant differences in fecal bacterial diversity (Figure S4A) and bacterial richness and evenness, assessed by Shannon and Simpson indices, respectively (Figure S4B). As expected, after breeding establishment, beta diversity analysis of the maternal fecal microbiota showed a significant change in bacterial diversity of $TCR\delta^{-/-}$ and $TCR\delta^{+/-}$ females before and after co-housing (Figures S4C and S4D); no changes in bacterial richness were observed (Figures S4E and S4F). As a result, after the establishment of breeding pairs, $TCR\delta^{-/-}$ and $TCR\delta^{+/-}$ dams displayed similar bacterial diversity and richness in their fecal (Figures S5A and S5B), vaginal (Figures S5C and S5D), and cutaneous (Figures 4A and 4B) microbiota. However, comparison of the relative abundances of specific skin microbial communities showed a significant increase of Bacteroidetes phyla and *Oscillospira* genus in $TCR\delta^{+/-}$ dams (Figures 4C and 4D) and a minor increase of *Parvimonas* and *Tannerella* genera in $TCR\delta^{-/-}$ dams (Figure 4C). Hence, even though the co-housing process largely homogenizes the microbiota, taxa-specific differences in the skin microbiota are retained between $TCR\delta^{+/-}$ and $TCR\delta^{-/-}$ dams. Given that γδ T cells often act through the secretion of cytokines and are major producers of IL-17A and IL-22,[34] both of which have been implicated in the regulation of commensal microbes,[35,36] we employed the reciprocal breeding strategy using $Il17a^{-/-}$ and $Il22^{-/-}$ mice in order to investigate if these cytokines were implicated in the regulation of neonatal pulmonary immune responses (Figures S6A and S6C). Surprisingly, and in clear contrast to what we observed in the progeny of the $TCR\delta^{-/-}$ dams (Figure 1E), the offspring of $Il17a^{-/-}$ and $Il22^{-/-}$ dams exhibited a decrease in the levels of lung IL-33 (Figures S6B and S6D), IL-5 (Figure S6B), and IL-12p40 (Figure S6D) when compared with the offspring of control dams. As an alternative mechanism, we next evaluated the expression of multiple antimicrobial peptides (AMPs)[35,37] in the skin of $TCR\delta^{+/-}$ and $TCR\delta^{-/-}$ dams. Interestingly, even though we observed no differences in the expression of the genes encoding S100 proteins (*S100a7*, *S100a8*, and *S100a9*), defensins (*Defb2* and *Defb4*), or Reg1 (*Reg1*), $TCR\delta^{-/-}$ dams showed significantly lower expression

(B) Data pooled from three independent litter swaps per maternal genotype; n = 18–21 mice per group. (C and D) Data pooled from three independent litters per maternal genotype; n = 35–7 mice per group. (E–G) Data from one litter per maternal genotype; n = 4–6 mice per group. (B, D, F, and G) Box-and-whisker plots display first and third quartiles and the median; whiskers are from each quartile to the minimum or maximum. Normality of the samples was assessed with D'Agostino Pearson normality test; statistical analysis was then performed using Student's t test or Mann-Whitney test. *p < 0.05.

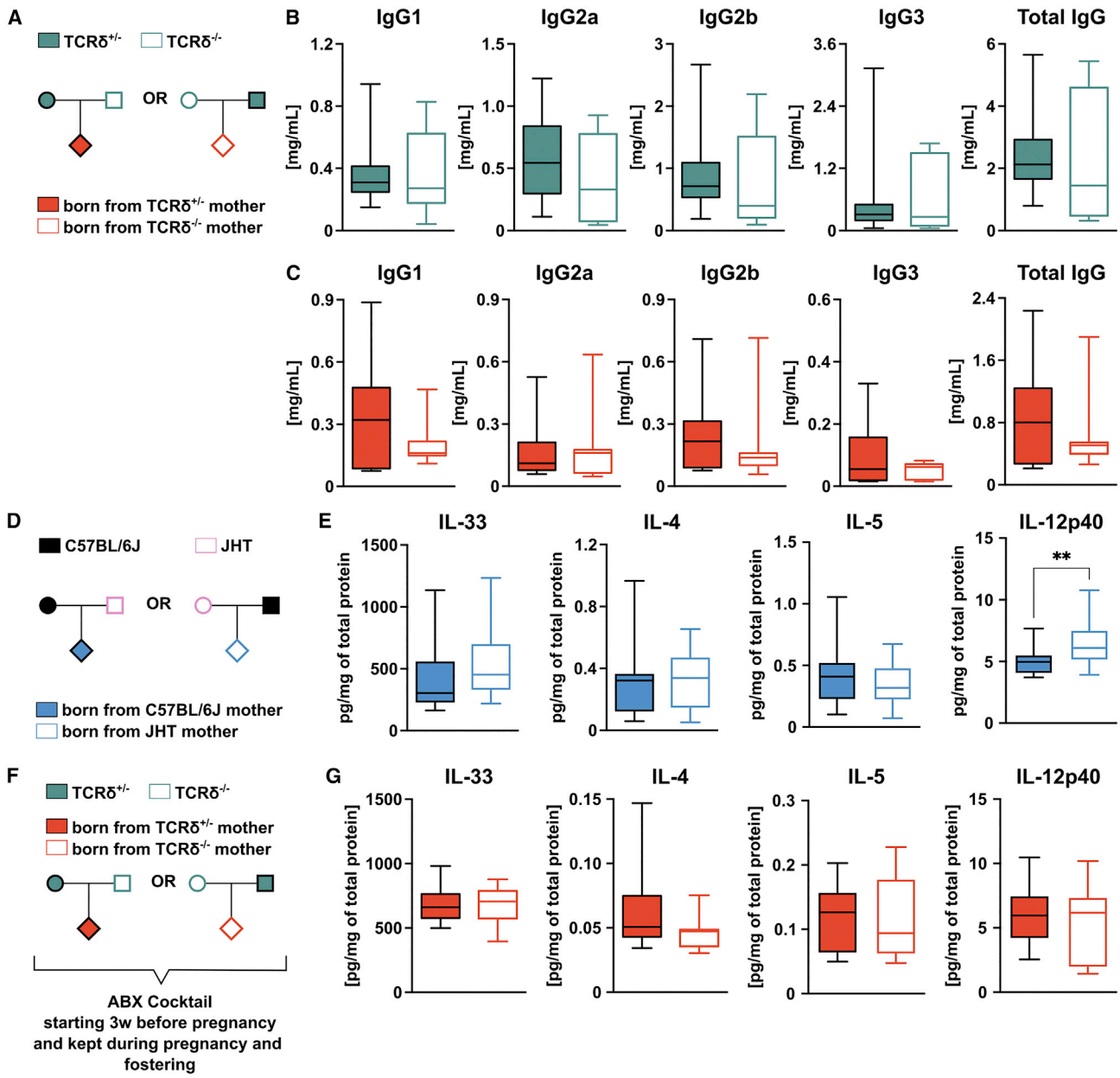

Figure 3. Maternal regulation of first-breath-induced inflammation in the offspring is microbiota dependent but antibody independent

(A) Breeding strategy.

(B and C) Concentration of total IgG and its subclasses in the serum of (B) *TCRδ*$^{+/-}$ and *TCRδ*$^{-/-}$ dams and their (C) progeny.

(D) Breeding strategy employed to evaluate if maternal transfer of antibodies impact on perinatal lung inflammation.

(E) Concentration of cytokines within the whole lung homogenate normalized by total protein, grouped by maternal genotype.

(F) Breeding strategy employed to evaluate the role of microbiota in mediating maternal γδ T cell conditioning of the pulmonary immune system of the offspring.

(G) Concentration of cytokines within the whole lung homogenate normalized by total protein, grouped by maternal genotype.

(B) n = 7–14 mice per group. (C) n = 19–21 mice per group. (E) n = 18–22 mice per group. (G) n = 17–18 mice per group. (C–G) Data pooled from three independent litters per maternal genotype. (B, C, E, and G) Box-and-whisker plots display first and third quartiles and the median; whiskers are from each quartile to the minimum or maximum. Normality of the samples was assessed with D'Agostino Pearson normality test; statistical analysis was then performed using Student's t test or Mann-Whitney test. **p < 0.01.

of *Reg3g* and *Gpr15l*, encoding the AMP Reg3-γ and GPR-15L, respectively (Figure 4E). Of note, we found no differences in the expression of AMP genes in vaginal tissue (Figure S7A). Thus, the regulation of particular AMPs, such as Reg3-γ and GPR-15L, selectively in the skin may explain how γδ T cells shape local commensal bacterial communities.

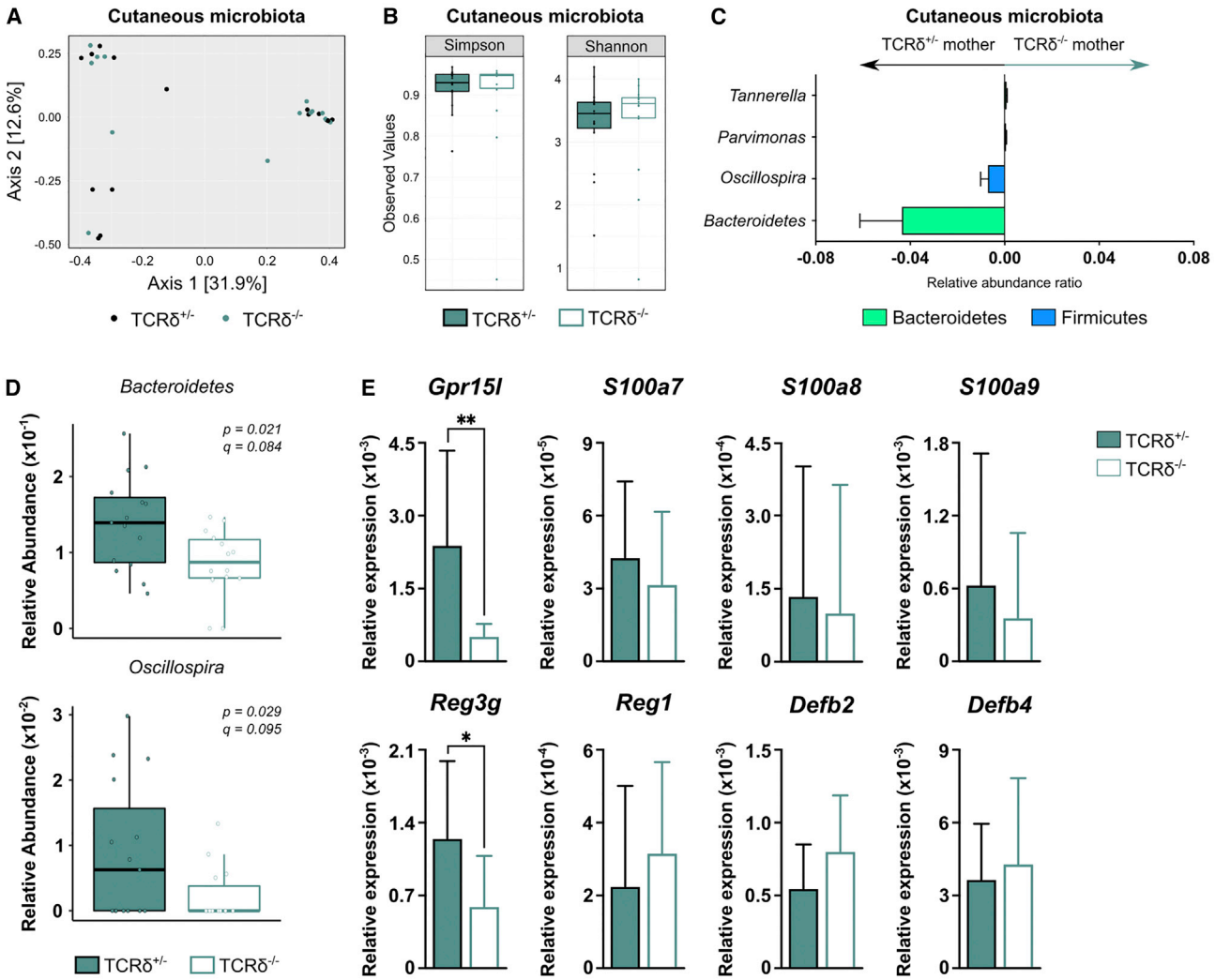

Figure 4. *TCRδ*$^{+/-}$ and *TCRδ*$^{-/-}$ dams display discrete skin microbiota and antimicrobial peptide profiles even after co-housing

(A and B) Microbial composition differences in skin microbiota from *TCRδ*$^{+/-}$ and *TCRδ*$^{-/-}$ dams are plotted using (A) beta diversity (Bray-Curtis dissimilarity principal-coordinate analysis [PCoA]) and (B) alpha diversity (Shannon and Simpson indices).

(C) Skin microbiota taxa associated with *TCRδ*$^{+/-}$ and *TCRδ*$^{-/-}$ dams and plotted as relative abundance ratios.

(D) Relative abundance of taxa significantly enriched ($p < 0.05$, $q < 0.2$) in the skin microbiota of *TCRδ*$^{+/-}$ dams.

(E) Gene expression of AMP genes in total skin tissue from *TCRδ*$^{+/-}$ and *TCRδ*$^{-/-}$ dams normalized to the average expression of *18S and Actb*.

(A–D) n = 14–15 mice per group. Box-and-whisker plots display first and third quartiles and whiskers are from each quartile to the minimum or maximum. (E) n = 10 mice per group. Error bars represent mean ± SD. Normality of the samples was assessed with D'Agostino Pearson normality test; statistical analysis was then performed using Student's t test or Mann-Whitney test. *$p < 0.05$; **$p < 0.01$.

The progeny of *TCRδ*$^{+/-}$ dams acquires postnatally an intestinal microbiota with increased capacity to produce SCFAs

Taken together, our data led us to hypothesize that the offspring of *TCRδ*$^{-/-}$ and *TCRδ*$^{+/-}$ dams are subjected to a distinct neonatal microbial colonization. While no differences were found in bacterial diversity and richness in the lung microbiota from the progeny of *TCRδ*$^{-/-}$ and *TCRδ*$^{+/-}$ dams (Figures S8A and S8B), analysis of the microbial composition of the cecal contents evidenced significant, albeit minor, differences in bacterial diversity (Figure 5A) and a decrease in bacterial richness in pups born from *TCRδ*$^{-/-}$ dams (Figure 5B). No differences in bacterial diversity or richness were found based on the genotype of the progeny (Figure S8C and S8D). Pups born from *TCRδ*$^{+/-}$ dams displayed significantly increased relative abundances in the genera *Rikenellaceae RC9 gut group*, *Muribaculaceae*, and *Lachnospiraceae UCG-006*. At the family level, the relative abundance of *Rikenellaceae*, *Muribaculaceae*, *Oscillospiraceae*, *Ruminococcaceae*, and *Erysipelatoclostridiaceae* was significantly higher in the offspring of *TCRδ*$^{+/-}$ dams (Figures 5C and S9C). Pups born from *TCRδ*$^{-/-}$ dams, on the other hand, displayed an increase in the genus *Lachnoclostridium* (Figures 5C and

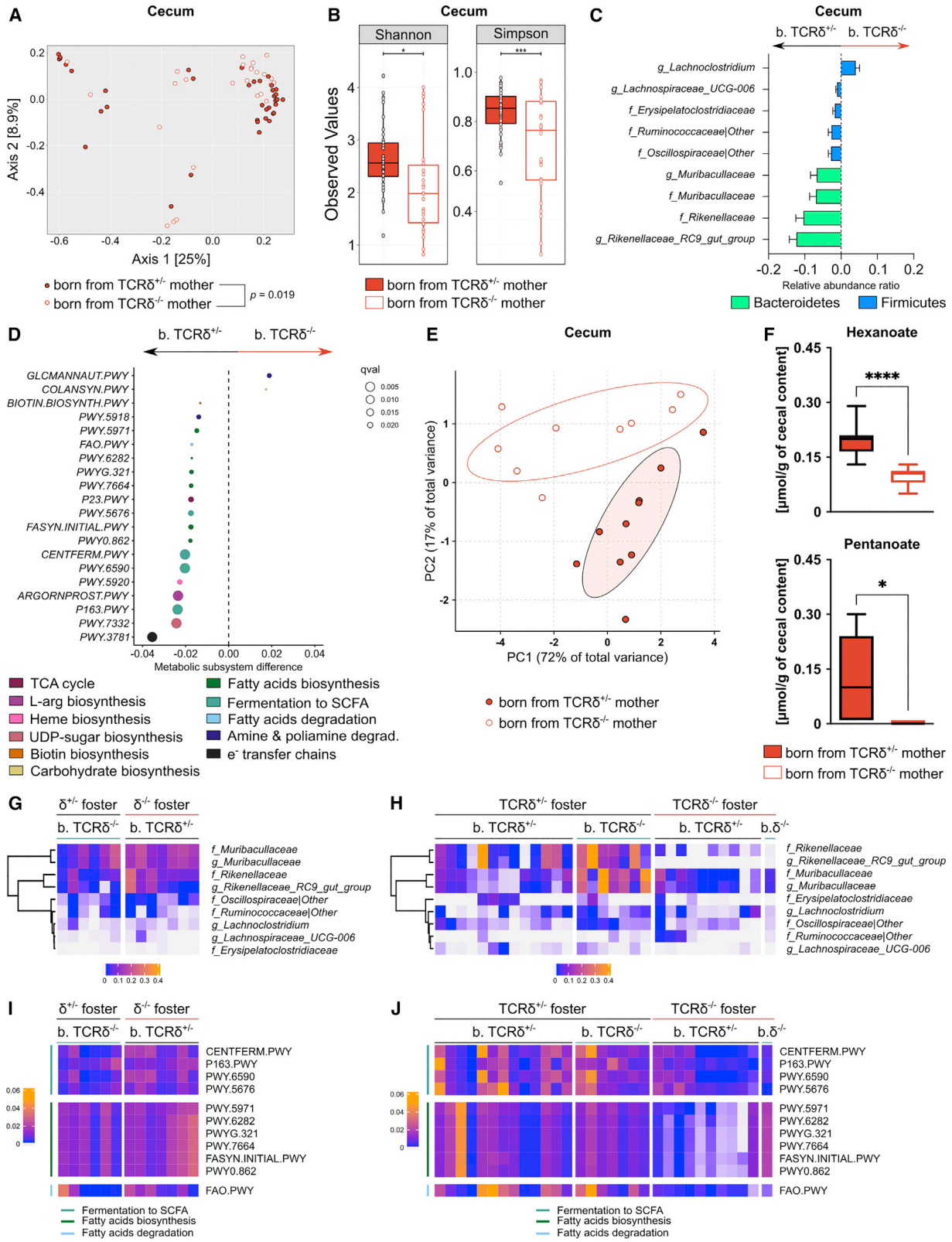

(legend on next page)

S8E). Most importantly, to evaluate the relevance of these taxonomy changes, we used the Phylogenetic Investigation of Communities by Reconstruction of Unobserved States (PICRUSt) pipeline to predict the functional metagenome of cecal bacterial communities found in the offspring of $TCR\delta^{-/-}$ and $TCR\delta^{+/-}$ dams.[38] Several metabolic pathways were predicted to be upregulated in the microbiota of pups born from $TCR\delta^{+/-}$ dams. Interestingly, the 20 most significantly different metabolic pathways were enriched for pathways comprising fatty acid biosynthesis and degradation and fermentation to SCFAs (Figure 5D). Corroborating our *in silico* predictions, analysis of cecum levels of SCFAs by gas chromatography-mass spectrometry showed a distinct SCFA profile for the progeny of $TCR\delta^{-/-}$ and $TCR\delta^{+/-}$ dams (Figure 5E), with pups born from $TCR\delta^{+/-}$ dams presenting increased levels of pentanoate and hexanoate and, although not statistically significant, a trend for increased levels of acetate ($p = 0.0506$); no differences were observed in other SCFAs measured (Figures 5F and S9F). Altogether, these results indicate that a differential neonatal intestinal bacterial colonization between pups born from $TCR\delta^{-/-}$ and $TCR\delta^{+/-}$ dams results in changes in the availability of microbial-derived metabolites, ultimately impacting on the first-breath-induced reaction.

Germane to our working hypothesis, given that cross-fostered and C-Sec-delivered pups showed no differences in lung type 2 immunity, we predicted that disruption of neonatal colonization by cross-fostering and C-Sec surgeries also abrogated the differences in bacterial composition and their metabolic potential. Indeed, we found no differences in intestinal bacterial richness in cross-fostered pups (Figure S9A), even though they still presented a significant difference in bacterial diversity (Figure S9B). For C-Sec-delivered pups we observed a more complex picture: the use of the Shannon index revealed no significant differences in bacterial richness between the analyzed C-Sec groups, irrespective of their birth or foster mother (Figure S9C); the Simpson index, however, shows small differences in bacterial evenness depending on the genotype of the foster mother (Figure S9C). Likewise, C-Sec-delivered pups still retained some significant differences in bacterial diversity, again mostly dependent on the genotype of the foster mother (Figure S9D). As expected, cross-fostering largely homogenized the top 30 most abundant taxa between the offspring of $TCR\delta^{-/-}$ and $TCR\delta^{+/-}$ dams; C-Sec delivery, on the other hand, was less consistent but suggested that some of the most represented taxa are acquired vertically after birth and are highly dependent on the genotype of the foster dam (Figure S9E). Taken together, the comparison of the microbiota from cross-fostered and C-Sec-delivered pups indicates that most bacterial communities are transferred postnatally, with some being seeded around birth and persisting even after a perturbation such as cross-fostering. Accordingly, when we focused our analysis specifically on the taxa found to be significantly different between the offspring of $TCR\delta^{-/-}$ and $TCR\delta^{+/-}$ dams, we observed that cross-fostering completely abrogated those differences (Figures 5G and S10A). Analysis of the microbiota from C-Sec-delivered pups showed that bacteria from the family *Rikenellaceae* and genus *Rikenellaceae RC9 gut group* are transferred during fostering and only by $TCR\delta^{+/-}$ dams (Figures 5H and S10B); all other significantly different bacterial communities, however, were found to be largely similar between groups, with the exception of bacteria from the family and genus *Muribaculaceae*, which were significantly increased in pups born from $TCR\delta^{-/-}$ dams via C-Sec and fostered by $TCR\delta^{+/-}$ mothers (Figures 5H and S10B). Finally, *in silico* prediction of microbial functionality confirmed that cross-fostering abrogated the differences in the metabolic pathways related to fatty acid biosynthesis and degradation and SCFA production observed in pups born from $TCR\delta^{-/-}$ and $TCR\delta^{+/-}$ dams (Figures 5I and S10C). Interestingly, C-Sec-delivered pups fostered by $TCR\delta^{+/-}$ dams retained the upregulation of pathways controlling fatty acid metabolism but lost the differences in the pathways related to SCFA production (Figures 5J and S10D). Given that bacteria from the families *Oscillospiraceae*, *Ruminococcaceae*, and *Erysipelatoclostridiaceae* and genus *Lachnospiraceae UCG-006* were significantly decreased in the progeny of $TCR\delta^{-/-}$ dams but equally distributed among cross-fostered and C-sec-delivered pups, we propose that these taxa are vertically transferred postnatally to the pups from $TCR\delta^{+/-}$ dams having a suppressive effect on neonatal lung type 2 immunity. Moreover, our data, together

Figure 5. The offspring of γδ-sufficient dams acquire postnatally a discrete gut microbiota with increased SCFA production compared with pups born from γδ-deficient dams

(A and B) Microbial composition differences in cecum microbiota from pups born from $TCR\delta^{+/-}$ and $TCR\delta^{-/-}$ dams are plotted using (A) beta diversity (Unifrac PCoA) and (B) alpha diversity (Shannon and Simpson indices).

(C) Cecum microbiota taxa associated with maternal genotypes ($p < 0.05$, $q < 0.05$) and plotted as relative abundance ratios.

(D) PICRUSt analysis of the neonatal cecum microbiota plotted as differentially regulated pathways associated with maternal genotype ($p < 0.05$, $q < 0.05$).

(E) Principal-component analysis (PCA) plot depicting the clustering of pups based on their cecal SCFA profile.

(F) Concentration of SCFAs present in the cecum of pups normalized by cecal content.

(G and H) Heatmap depicting the relative abundance ratios for the selected taxa in (G) cross-fostered pups and (H) C-Sec-delivered pups associated with maternal genotypes.

(I and J) Heatmap depicting the selected metabolic pathways associated with maternal genotype in (I) cross-fostered pups and (J) C-Sec-delivered pups associated with maternal genotype.

(A–D) Data pooled from two independent litters per maternal genotype; n = 38–26 mice per group. (E and F) Data from one litter per maternal genotype; n = 9–10 mice per group. (G–J) Data pooled from at least two independent litters per maternal genotype; n = 13–7 mice per group (with the exception of the group of pups born from $TCR\delta^{-/-}$ via C-Sec and fostered by a mother of the same genotype, where only one pup survived the procedure). (C) Error bars represent mean ± SD; statistical analyses for taxonomy and PICRUSt results were performed using the MaAsLin pipeline with Benjamini-Hochberg false discovery rate (BH-FDR) (q value) $q < 0.05$ and $p < 0.05$ being considered significant. (F) Box-and-whisker plots display first and third quartiles and the median; whiskers are from each quartile to the minimum or maximum; normality of the samples was assessed with D'Agostino Pearson normality test; statistical analysis was then performed using Student's t test or Mann-Whitney test. *$p < 0.05$; ***$p < 0.001$; ****$p < 0.0001$. b., born from.

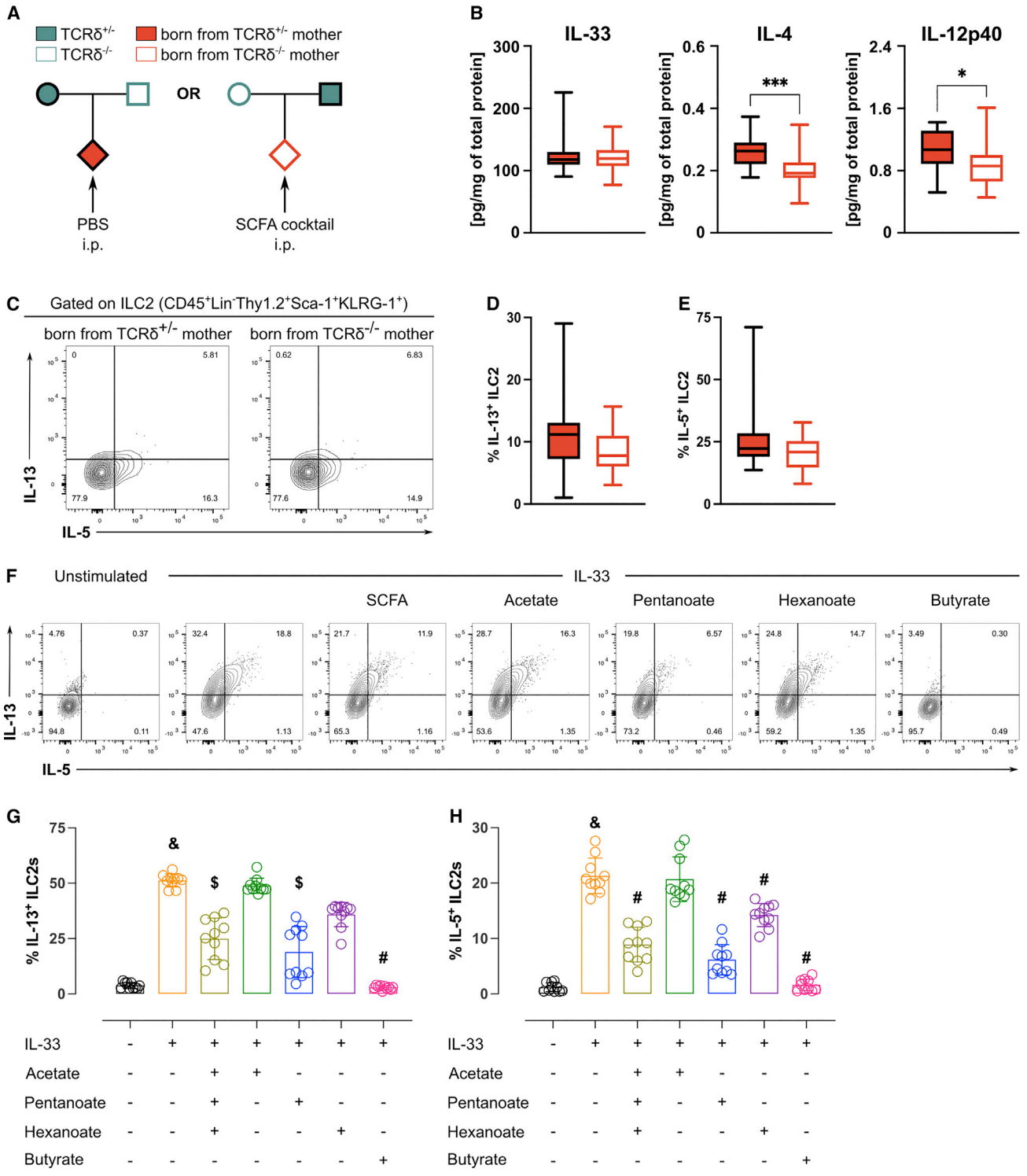

Figure 6. Microbiota-derived SCFAs in the offspring suppress exacerbated perinatal type 2 inflammatory responses in the lung

(A) Breeding strategy employed to evaluate the role of SCFAs in regulating perinatal lung inflammation.

(B) Concentration of cytokines within the whole lung homogenate normalized by total protein, grouped by maternal genotype.

(C) Flow cytometry analysis of intracellular IL-5 and IL-13 in ILC2s isolated from the lungs and stimulated *in vitro* for 3 h in the presence of PMA, ionomycin, and brefeldin A.

(D and E) Frequencies of (D) IL-13^{+} and (E) IL-5^{+} cells within the ILC2 population in the lungs of pups depicted in (A), grouped by maternal genotype.

(legend continued on next page)

with reports from the literature,[39,40] link these taxa to SCFA production, suggesting that these microbial-derived metabolites may mediate the proposed regulatory gut-lung axis.

Microbial-derived SCFAs prevent exacerbated pulmonary first-breath-induced type 2 inflammation and control postweaning response to helminth infection

In order to test if exogenous SCFA supplementation was sufficient to suppress the increased type 2 activation observed in the lungs of pups born from γδ T cell-deficient dams, we administered an SCFA cocktail to the offspring of *TCRδ*$^{-/-}$ dams (Figure 6A). Confirming our hypothesis, administration of the SCFA cocktail to pups born from *TCRδ*$^{-/-}$ dams abrogated the differences observed in the tissue levels of IL-33 while significantly decreasing IL-4 and IL-12p40 concentrations (Figure 6B). Moreover, the treatment also downregulated ILC2 activation and function in the offspring of *TCRδ*$^{-/-}$ dams, as evidenced by similar frequencies of IL-13^{+} and IL-5^{+} cells (Figures 6C–6E). Importantly, administration of the SCFA cocktail via drinking water to *TCRδ*$^{-/-}$ dams was not sufficient to decrease the frequencies of IL-13- and IL-5-producing ILC2 in their progeny when compared with that of their *TCRδ*$^{+/-}$ counterparts (Figures S11A–S11D); lung levels of IL-33 were also still higher in pups born from *TCRδ*$^{-/-}$ dams (Figure S11E). In order to increase our mechanistic understanding of how SCFAs regulated type 2 immunity, we employed an *in vitro* system to restimulate purified ILC2s with IL-33 in the presence of the SCFA cocktail, its individual components, or butyrate as a positive control for ILC2 suppression.[41] Corroborating our *in vivo* data, the addition of the SCFA cocktail to IL-33-stimulated ILC2s decreased the production of IL-13 and IL-5 (Figures 6F–6H). Moreover, addition of pentanoate alone was sufficient to recapitulate the effects of the full cocktail (Figures 6F–6H); hexanoate, on the other hand, significantly decreases IL-5 production but not IL-13 (Figures 6F–6H). Notably, no differences in cytokine production were observed upon the addition of acetate (Figures 6F–6H). Altogether, these findings suggest that bacterial-derived SCFAs as inferred from the microbial consortial analysis, in particular pentanoate and hexanoate, regulate the first-breath reaction by directly suppressing ILC2 cytokine production.

The increase in first-breath-induced type-2 inflammation in the pups born from γδ T cell-deficient dams, together with our initial results using the *N. brasiliensis* infection model, prompted us to further investigate how the offspring of *TCRδ*$^{-/-}$ dams would respond to a type 2-promoting insult. In order to address this question, mice were infected at the postweaning period with *N. brasiliensis* (Figure 7A). Although we did not observe differences in lung damage at day 2 or 6 postinfection (p.i.) or in gut worm burden at day 6 p.i. (Figures S12A–S12C), mice born from *TCRδ*$^{-/-}$ dams presented an increased inflammatory response to the infection when compared with the offspring of γδ T cell-sufficient dams, characterized by higher numbers of total leukocytes infiltrating the lung (Figure 7B) and enhanced eosinophilia and neutrophilia (Figures 7C and 7D). Surface expression of programmed cell death-ligand 2 (PD-L2) in macrophages and dendritic cells (DCs) has been reported to occur under strong type 2 conditions.[42,43] Accordingly, we observed increased numbers of PD-L2-expressing macrophages (Figures 7E and 7F) and DCs (Figures 7G and 7H) in mice born from *TCRδ*$^{-/-}$ dams when compared with controls. In line with these results, we also found an increase in IL-13^{+} and IL-17A^{+} (but not interferon γ [IFN-γ]$^{+}$) CD4^{+} T cells (Figures 7I and 7J) in the progeny of *TCRδ*$^{-/-}$ dams. When mice were categorized according to their own genotype, we observed no differences between *TCRδ*$^{-/-}$ and *TCRδ*$^{+/-}$ animals in any of the aforementioned parameters (Figures S12D–S12I). Taken together, we have found that the offspring of *TCRδ*$^{-/-}$ dams display stronger type 2 immune responses, irrespective of their own genotype, both in steady state and upon an infectious challenge.

Next, we sought to evaluate if SCFA supplementation preweaning would also be able to suppress the increased inflammatory response during helminth infection observed in the progeny of *TCRδ*$^{-/-}$ dams (Figures 7A–7J). Therefore, we infected with *N. brasiliensis* SCFA-treated mice, born from *TCRδ*$^{-/-}$ dams, together with vehicle-treated mice, born from *TCRδ*$^{+/-}$ dams (Figure 7K). Critically, upon SCFA administration, the offspring of *TCRδ*$^{-/-}$ dams showed no differences, when compared with controls, in the numbers of total leukocytes (Figure 7L), neutrophils (Figure 7M), and eosinophils (Figure 7N) infiltrating the lung upon infection. Furthermore, we also found the number of infection-induced PD-L2-expressing macrophages (Figure 7O) and DCs (Figure 7P) to be similar between mice born from *TCRδ*$^{-/-}$ and *TCRδ*$^{+/-}$ dams. Finally, after SCFA supplementation, the progeny of *TCRδ*$^{-/-}$ dams presented similar frequencies of lung IL-13^{+}, IL17^{+}, and IFN-γ^{+} CD4^{+} T cells in response to *N. brasiliensis* infection when compared with mice born from *TCRδ*$^{+/-}$ dams (Figure 7Q). Taken together, our data ascribe the phenotypes observed in the *TCRδ*$^{-/-}$ progeny to decreased maternal transfer of SCFA-producing bacteria, which, beyond increasing first-breath-induced type 2 inflammation, exacerbates inflammatory responses to helminth infection after weaning.

DISCUSSION

Non-heritable factors, including the microbiome, are perceived as major contributors to systems physiology and immune

(F–H) ILC2s were electronically sorted, plated, and restimulated for 24 h *in vitro* with the conditions depicted.
(F) Representative fluorescence-activated cell sorting (FACS) plots showing IL-5 and IL-13 production.
(G and H) Quantification of (G) IL-13^{+} and (H) IL-5^{+} ILC2s.
(B–E) Data pooled from three independent litters per maternal genotype; n = 17–18 mice per group. (F–H) Data pooled from two independent sorting sessions with 5 C57Bl6/J mice pooled per experiment; n = 10 mice per group. (B, D, and E) Box-and-whisker plots display first and third quartiles and the median; whiskers are from each quartile to the minimum or maximum; (G–H) Each symbol represents a replicate; error bars represent mean ± SD. Normality of the samples was assessed with D'Agostino Pearson normality test; statistical analysis was then performed using Student's t test or Mann-Whitney test. *p < 0.05; ***p < 0.001; ****p < 0.0001. (F–H) &p < 0.0001 when compared with non-stimulated control; $p < 0.01 when compared with IL-33-stimulated control; #p < 0.0001 when compared with IL-33-stimulated control.

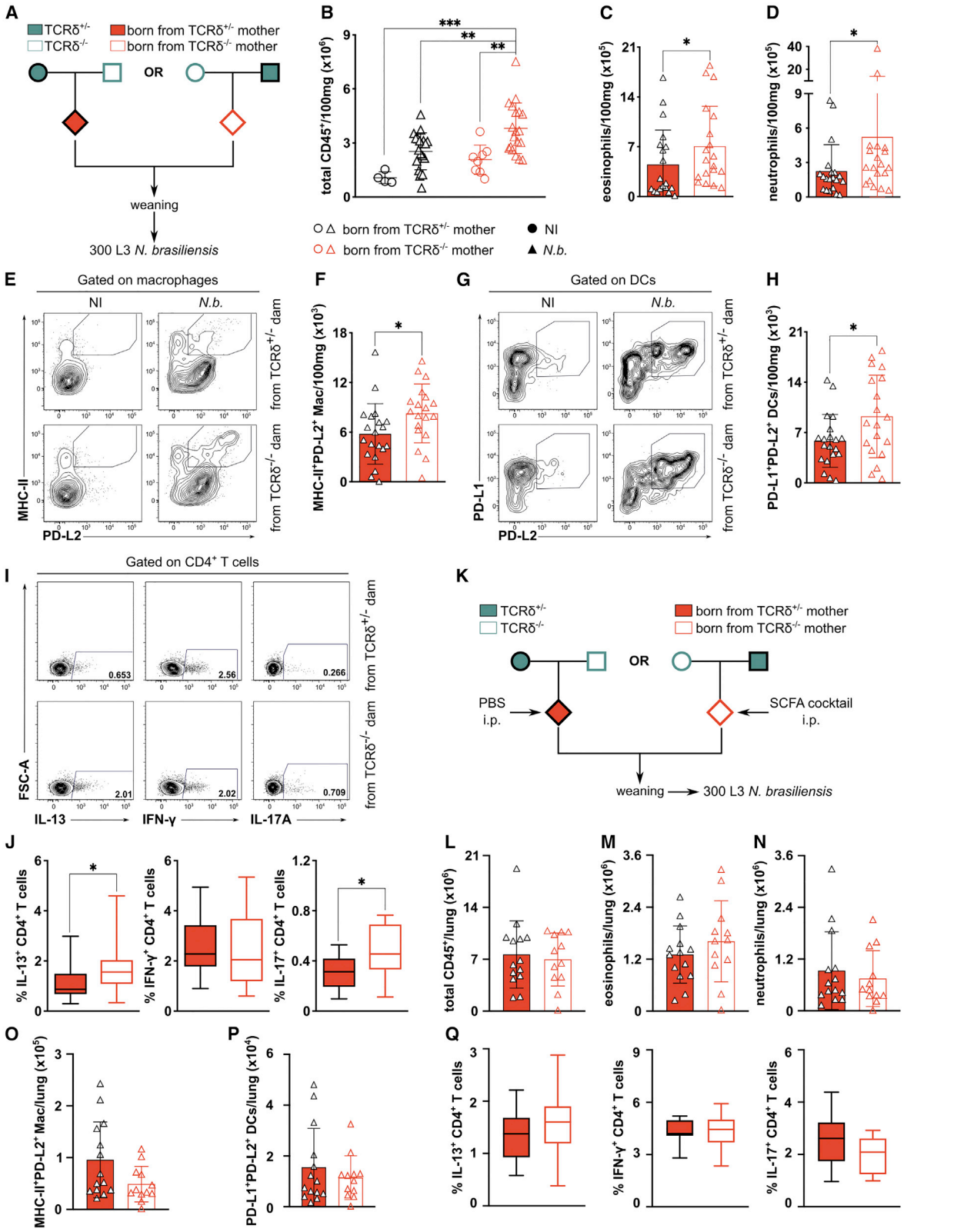

(legend on next page)

variation in healthy humans.[11,44] In mice, many changes in cellular and humoral immune responses have been demonstrated to be microbiota dependent.[45,46] While this makes the design of experiments aimed at evaluating gene-intrinsic effects on a given phenotype more complex, it can be resolved by the use of littermate controls.[11] Despite being considered "gold standard," this practice it is still not common in biomedical research; in particular, in the field of γδ T cells and infectious diseases, only about 15% of the published studies since the development of *TCRδ*$^{-/-}$ mice (1993) have used littermate controls over the years (Figures S13A and S13B), including a notable absence from top-ranked journals (Figure S13C). This may be the basis of some of the inconsistencies reported over the years regarding the role of γδ T cells in lung immunity.

The fact that mice from the *TCRδ*$^{-/-}$ colony had a very different fecal microbiota, when compared with their counterparts coming from the *TCRδ*$^{+/-}$ colony, was striking: first, because the heterozygous breeding was established with founder animals from the *TCRδ*$^{-/-}$ colony, and second, because both mouse lines were kept under the same selective environmental pressures. Interestingly, Krishnan et al.[25] reported significant differences in the oral microbiota of *TCRδ*$^{-/-}$ mice when compared with genetic background-matched C57BL/6J mice. Moreover, using a model for acute depletion of γδ T cells, Wilharm et al.[26] found that continuous ablation of γδ T cells induces profound changes in the oral microbiome compared with control (non-depleted) animals. Altogether, these data suggest that γδ T cells—found in abundant numbers at barrier tissues—actively select bacterial commensals and could explain our findings that, even after co-housing, *TCRδ*$^{-/-}$ dams retain differences in cutaneous bacterial communities. This is in line with evidence that co-housing does not equalize niche-specific microbiota within the intestines of genetically identical mice.[47] As we observed persisting differences in cutaneous bacterial communities in *TCRδ*$^{-/-}$ dams alongside decreased expression of the AMPs *Gpr15l* and *Reg3g*, we propose that γδ T cells may shape skin microbiota through AMP regulation in a process that is independent of IL-17A and IL-22. Of note, AMPs have already been shown to shape the microbiota.[24,48,37] In our system, this seems to be tissue specific, as we did not observe differences in the microbiota or AMP expression in the female reproductive tract of *TCRδ*$^{-/-}$ mice. Importantly, GPR15L has been shown to be critical for the maintenance of dendritic epidermal T cells (DETCs; Lahl et al., 2014[49]), a major γδ T cell population in the skin, and disruption of this axis in *GPR15*$^{-/-}$ mice leads to skin dysbiosis.[50]

Previous analysis of human mother-infant pairs corroborates our results, showing that maternal skin and vaginal strains transferred perinatally start the earlier colonization, followed by gut-derived strains.[51] The results we obtained from our cross-fostering and C-Sec experiments indicate that most bacterial communities found to be increased in the offspring of *TCRδ*$^{+/-}$ dams were transferred postbirth. Furthermore, although some metabolic pathways remained different between the pups delivered by C-Sec from *TCRδ*$^{-/-}$ or *TCRδ*$^{+/-}$ dams, we observed an equalization of the pathways associated with the production of SCFAs. Thus, our results seem to indicate that the period comprising delivery and the few following days are crucial not only to determine the microbiota composition but also its functional capacity. While our results do not directly show which maternal compartment provides the pioneering bacterial communities, our data suggest that the skin of *TCRδ*$^{-/-}$ and *TCRδ*$^{+/-}$ dams display differences that may influence neonatal gut colonization and ultimately regulate the first-breath-induced pulmonary reaction.

Even though rodent pulmonary immune system development starts during fetal life,[52] the main changes occur during the first 2 weeks of life. Changing from a fluid-filled to an air-filled environment entails sustained basal type 2 immune responses—a critical feature to keep organ function during this heavy remodeling phase.[9,10] Our results indicate that early-life gut-colonizing microbes and their metabolites are able to fine-tune this lung type 2 activation, indicating that the process of IL-33 release by airway epithelial cells involves more than physical stress.[10] To date, little was known about the effects of pentanoate and hexanoate on type 2 immune responses. Reports in the literature indicate that pentanoate can present both suppressive and enhancing effects on lymphocytes either by reducing IL-17 production in CD4$^+$ T cells[53] or inducing IFN-γ production in CD8$^+$ T cells.[54] Our *in vivo* and *in vitro* approach

Figure 7. SCFAs control exacerbated response to *N. brasiliensis* infection in the offspring of γδ T cell-deficient dams

(A) Breeding strategy employed to evaluate the gene-extrinsic and -intrinsic roles of γδ T cell depletion on pulmonary immunity.

(B–D) Numbers of (B) total leukocytes, (C) eosinophils, and (D) neutrophils in mice described in (A).

(E) Flow cytometry analysis of surface major histocompatibility complex (MHC) class II and PD-L2 expression in lung macrophages (defined as CD45$^+$CD64$^+$CD24$^-$ live cells).

(F) Numbers of MHC class II$^+$PD-L2$^+$ macrophages in the lungs.

(G) Flow cytometry analysis of surface PD-L1 and PD-L2 expression in lung dendritic cells (DCs; defined as CD45$^+$CD64$^-$CD24$^+$CD11c$^+$MHC class II$^+$ live cells) isolated from the lungs.

(H) Numbers of PD-L1$^+$PD-L2$^+$ DCs in the lungs.

(I and J) Flow cytometry analysis of IL-13$^+$, IFN-γ$^+$, and IL-17A$^+$ CD4$^+$ (I) and their frequencies (J) in the lungs.

(K) Breeding strategy employed to evaluate the role of SCFAs on regulation of offspring pulmonary immunity.

(L–P) Numbers of (L) total leukocytes, (M) eosinophils, (N) neutrophils, (O) MHC class II$^+$PD-L2$^+$ macrophages, and (P) PD-L1$^+$PD-L2$^+$ DCs in the lungs of mice described in (K).

(Q) Frequencies of IL-13$^+$, IFN-γ$^+$, and IL-17A$^+$ CD4$^+$ T cells in the lungs of mice described in (K).

Data pooled from three independent litters per genotype. (B–J) n = 14–16 mice per group. (L–P) n = 12–14 mice per group. (B–D, F, H, and L–P) Each symbol represents an individual mouse. Error bars represent mean ± SD. (J and Q) Box-and-whisker plots display first and third quartiles and the median; whiskers are from each quartile to the minimum or maximum. Normality of the samples was assessed with D'Agostino Pearson normality test; statistical analysis was then performed using Student's t test or Mann-Whitney test. *$p < 0.05$; **$p < 0.01$; ***$p < 0.001$.

demonstrated that pentanoate (and to a lesser extent hexanoate) is also able to directly suppress ILC2 activation and cytokine production. In addition, it is important to note that for the intestinal immune system, the action of SCFAs seems to occur at the time of weaning.[3] In our study, however, we show that lung immunity is affected by microbiota-derived SCFAs before weaning, and *in utero* transfer of SCFAs was not responsible for the regulation of lung type 2 immunity in the offspring of *TCRδ*$^{-/-}$ dams. These findings underscore the discrete maturation time windows for the immune cells residing within different tissues and the context-specific effects of SCFAs.

While nutrition, especially during pregnancy and breast feeding, has a major impact on early microbiota composition and offspring physiology,[7,12,55] our study highlights the importance of microbiota transmission from mother to infant at the perinatal stage[51] to the establishment of gut microbiota functionality, which conditions the physiology of a distant organ, the lung, undergoing major immune remodeling during early life.

Limitations of the study

Our data suggest that maternal γδ T cells regulate postnatal microbial colonization and microbial-derived metabolite availability in the offspring, ultimately impacting the pulmonary immune system development. Even though we observed the presence of different bacterial taxa in the skin of *TCRδ*$^{-/-}$ and *TCRδ*$^{+/-}$ dams even after co-housing, together with tissue-specific differences in the expression of AMP genes, we could not pinpoint the mechanism by which γδ T cells might change microbiota composition. Moreover, our data do not allow us to fully determine from which maternal compartment the pioneering bacterial communities are coming from. As γδ T cells are found in relatively high numbers in the female reproductive tract, it was somewhat surprising to observe no differences in either the microbiota or the expression of AMPs in vaginal tissue from *TCRδ*$^{-/-}$ and *TCRδ*$^{+/-}$ dams. However, a caveat is that the vaginal tissue used for both 16S sequencing or gene expression analysis was not obtained from pregnant females just before birth. Maternal vaginal microbiota changes significantly during gestation, with a particularly dramatic change happening during the late phases of pregnancy and at birth,[56] thus raising the possibility that the absence of γδ T cells might differentially impact the pre-partum changes in the microbiota. Finally, future studies should address the temporal scale that γδ T cells (and other immune cells) require to stably modify the microbiota.

STAR★METHODS

Detailed methods are provided in the online version of this paper and include the following:

- KEY RESOURCES TABLE
- RESOURCE AVAILABILITY
  - Lead contact
  - Materials availability
  - Data and code availability
- EXPERIMENTAL MODEL AND SUBJECT DETAILS
  - Mice and breeding setups
  - Study approval
- METHOD DETAILS
  - Cross-fostering and C-Sec surgeries
  - Cell preparation, flow cytometry, and analysis
  - In-vitro ILC2 stimulation
  - Immuno-detection of cytokines in lung tissue samples
  - Immuno-detection of antibodies in serum samples
  - RNA isolation, cDNA preparation and real-time PCR
  - N. brasiliensis *infection*
  - Histology and histopathological analysis
  - Antibiotic treatment and SCFA supplementation
  - Microbiota profiling via 16S rRNA gene sequencing
  - SCFA measurement
  - Literature review
- QUANTIFICATION AND STATISTICAL ANALYSIS
  - Statistical analysis

SUPPLEMENTAL INFORMATION

Supplemental information can be found online at https://doi.org/10.1016/j.celrep.2023.112074.

ACKNOWLEDGMENTS

We thank the precious technical assistance of the staff of iMM's Rodent Facility—especially Iolanda Moreira, Pedro Santos, and Bruno Novais—and the Flow Cytometry Unit. Thanks should also go to the staff at the Biological Services Facility and Flow Cytometry Facility at The University of Manchester. We are also grateful to the Rodent Facility and Genomics Unit of Instituto Gulbenkian de Ciência and MS-Omics for the services provided. We thank Marc Veldhoen for critical reading of the manuscript and Debanjan Mukherjee, Helena Brigas, Julie C. Ribot, Karine Serre, Ana Pamplona, Julie Darrigues,[57] Julie Chesné, Vânia Cardoso, Henrique Veiga-Fernandes (Champalimaud Center for the Unknown), James Parkinson (University of Manchester), and Ziad Al Nabhani (University of Bern) for helpful discussions and technical advice. This work was funded by Fundação para a Ciência e a Tecnologia (PTDC/MED-ONC/6829/2020 to B.S.-S.); European Molecular Biology Organization (LTF 191-2019 to P.H.P. and ALTF 252-2017 to G.J.F.); European Commission Marie Sklodowska-Curie Individual Fellowship (refs. 101025781 to P.H.P. and 752932 to G.J.F.); a Swiss National Foundation (SNF) Ambizione Grant (PZ00P3_185880 to B.Y.); the Novartis Foundation for Medical-Biological Research (#19A013 to B.Y.); the Sir Henry Dale Fellowship jointly funded by the Wellcome Trust and the Royal Society (105644/Z/14/Z to M.R.H.); the BBSRC (BB/T014482/1 to M.R.H.); and the Wellcome Trust (106898/A/15/Z to J.E.A.).

AUTHOR CONTRIBUTIONS

Conceptualization, P.H.P. and B.S.-S.; methodology and investigation, B.Y., G.P., S.M., C.C., G.J.F., D.G.d.C., N.G.-S., B.H.K.C., B.B., R.G.D., T.C., M.R.H., A.J.M., and J.E.A.; data analysis, P.H.P., B.Y., and G.P.; resources, B.H.K.C. and J.E.A.; writing – original draft, P.H.P. and B.S.-S.; writing – review & editing, P.H.P., B.Y., J.E.A., and B.S.-S.

DECLARATION OF INTERESTS

The authors declare no competing interests.

Received: August 5, 2021
Revised: December 21, 2022
Accepted: January 23, 2023
Published: February 13, 2023

REFERENCES

1. Brodin, P. (2022). Immune-microbe interactions early in life: a determinant of health and disease long term. Science *376*, 945–950. https://doi.org/10.1126/science.abk2189.
2. Tanaka, M., and Nakayama, J. (2017). Development of the gut microbiota in infancy and its impact on health in later life. Allergol. Int. *66*, 515–522. https://doi.org/10.1016/j.alit.2017.07.010.
3. Al Nabhani, Z., Dulauroy, S., Marques, R., Cousu, C., Al Bounny, S., Déjardin, F., Sparwasser, T., Bérard, M., Cerf-Bensussan, N., and Eberl, G. (2019). A weaning reaction to microbiota is required for resistance to immunopathologies in the adult. Immunity *50*, 1276–1288.e5. https://doi.org/10.1016/j.immuni.2019.02.014.
4. Wampach, L., Heintz-Buschart, A., Fritz, J.V., Ramiro-Garcia, J., Habier, J., Herold, M., Narayanasamy, S., Kaysen, A., Hogan, A.H., Bindl, L., et al. (2018). Birth mode is associated with earliest strain-conferred gut microbiome functions and immunostimulatory potential. Nat. Commun. *9*, 5091. https://doi.org/10.1038/s41467-018-07631-x.
5. Gomez de Agüero, M., Ganal-Vonarburg, S.C., Fuhrer, T., Rupp, S., Uchimura, Y., Li, H., Steinert, A., Heikenwalder, M., Hapfelmeier, S., Sauer, U., et al. (2016). The maternal microbiota drives early postnatal innate immune development. Science *351*, 1296–1302. https://doi.org/10.1126/science.aad2571.
6. Ramanan, D., Sefik, E., Galván-Peña, S., Wu, M., Yang, L., Yang, Z., Kostic, A., Golovkina, T.V., Kasper, D.L., Mathis, D., and Benoist, C. (2020). An immunologic mode of multigenerational transmission governs a. Cell *181*, 1276–1290.e13. https://doi.org/10.1016/j.cell.2020.04.030.
7. Thorburn, A.N., McKenzie, C.I., Shen, S., Stanley, D., Macia, L., Mason, L.J., Roberts, L.K., Wong, C.H.Y., Shim, R., Robert, R., et al. (2015). Evidence that asthma is a developmental origin disease influenced by maternal diet and bacterial metabolites. Nat. Commun. *6*, 7320. https://doi.org/10.1038/ncomms8320.
8. Renz, H., and Skevaki, C. (2021). Early life microbial exposures and allergy risks: opportunities for prevention. Nat. Rev. Immunol. *21*, 177–191. https://doi.org/10.1038/s41577-020-00420-y.
9. de Kleer, I.M., Kool, M., de Bruijn, M.J.W., Willart, M., van Moorleghem, J., Schuijs, M.J., Plantinga, M., Beyaert, R., Hams, E., Fallon, P.G., et al. (2016). Perinatal activation of the interleukin-33 pathway promotes type 2 immunity in the developing lung. Immunity *45*, 1285–1298. https://doi.org/10.1016/j.immuni.2016.10.031.
10. Saluzzo, S., Gorki, A.D., Rana, B.M.J., Martins, R., Scanlon, S., Starkl, P., Lakovits, K., Hladik, A., Korosec, A., Sharif, O., et al. (2017). First-breath-induced type 2 pathways shape the lung immune environment. Cell Rep. *18*, 1893–1905. https://doi.org/10.1016/j.celrep.2017.01.071.
11. Stappenbeck, T.S., and Virgin, H.W. (2016). Accounting for reciprocal host-microbiome interactions in experimental science. Nature *534*, 191–199. https://doi.org/10.1038/nature18285.
12. Kimura, I., Miyamoto, J., Ohue-Kitano, R., Watanabe, K., Yamada, T., Onuki, M., Aoki, R., Isobe, Y., Kashihara, D., Inoue, D., et al. (2020). Maternal gut microbiota in pregnancy influences offspring metabolic phenotype in mice. Science *367*, eaaw8429. https://doi.org/10.1126/science.aaw8429.
13. Macpherson, A.J., de Agüero, M.G., and Ganal-Vonarburg, S.C. (2017). How nutrition and the maternal microbiota shape the neonatal immune system. Nat. Rev. Immunol. *17*, 508–517. https://doi.org/10.1038/nri.2017.58.
14. Perez, M.F., and Lehner, B. (2019). Intergenerational and transgenerational epigenetic inheritance in animals. Nat. Cell Biol. *21*, 143–151. https://doi.org/10.1038/s41556-018-0242-9.
15. Itohara, S., Farr, A.G., Lafaille, J.J., Bonneville, M., Takagaki, Y., Haas, W., and Tonegawa, S. (1990). Homing of a gamma delta thymocyte subset with homogeneous T-cell receptors to mucosal epithelia. Nature *343*, 754–757. https://doi.org/10.1038/343754a0.
16. Pinget, G.V., Corpuz, T.M., Stolp, J., Lousberg, E.L., Diener, K.R., Robertson, S.A., Sprent, J., and Webster, K.E. (2016). The majority of murine gammadelta T cells at the maternal-fetal interface in pregnancy produce IL-17. Immunol. Cell Biol. *94*, 623–630. https://doi.org/10.1038/icb.2016.48.
17. Monin, L., Ushakov, D.S., Arnesen, H., Bah, N., Jandke, A., Muñoz-Ruiz, M., Carvalho, J., Joseph, S., Almeida, B.C., Green, M.J., et al. (2020). Gammadelta T cells compose a developmentally regulated intrauterine population and protect against vaginal candidiasis. Mucosal Immunol. *13*, 969–981. https://doi.org/10.1038/s41385-020-0305-7.
18. Koning, F., Stingl, G., Yokoyama, W.M., Yamada, H., Maloy, W.L., Tschachler, E., Shevach, E.M., and Coligan, J.E. (1987). Identification of a T3-associated gamma delta T cell receptor on Thy-1+ dendritic epidermal Cell lines. Science *236*, 834–837. https://doi.org/10.1126/science.2883729.
19. Nielsen, M.M., Witherden, D.A., and Havran, W.L. (2017). Gammadelta T cells in homeostasis and host defence of epithelial barrier tissues. Nat. Rev. Immunol. *17*, 733–745. https://doi.org/10.1038/nri.2017.101.
20. Reardon, C., Lefrancois, L., Farr, A., Kubo, R., O'Brien, R., and Born, W. (1990). Expression of gamma/delta T cell receptors on lymphocytes from the lactating mammary gland. J. Exp. Med. *172*, 1263–1266. https://doi.org/10.1084/jem.172.4.1263.
21. Fujihashi, K., McGhee, J.R., Kweon, M.N., Cooper, M.D., Tonegawa, S., Takahashi, I., Hiroi, T., Mestecky, J., and Kiyono, H. (1996). gamma/delta T cell-deficient mice have impaired mucosal immunoglobulin A responses. J. Exp. Med. *183*, 1929–1935. https://doi.org/10.1084/jem.183.4.1929.
22. Rezende, R.M., Lanser, A.J., Rubino, S., Kuhn, C., Skillin, N., Moreira, T.G., Liu, S., Gabriely, G., David, B.A., Menezes, G.B., and Weiner, H.L. (2018). Gammadelta T cells control humoral immune response by inducing T follicular helper cell differentiation. Nat. Commun. *9*, 3151. https://doi.org/10.1038/s41467-018-05487-9.
23. Khairallah, C., Chu, T.H., and Sheridan, B.S. (2018). Tissue adaptations of memory and tissue-resident gamma delta T cells. Front. Immunol. *9*, 2636. https://doi.org/10.3389/fimmu.2018.02636.
24. Papotto, P.H., Yilmaz, B., and Silva-Santos, B. (2021). Crosstalk between gammadelta T cells and the microbiota. Nat. Microbiol. *6*, 1110–1117. https://doi.org/10.1038/s41564-021-00948-2.
25. Krishnan, S., Prise, I.E., Wemyss, K., Schenck, L.P., Bridgeman, H.M., McClure, F.A., Zangerle-Murray, T., O'Boyle, C., Barbera, T.A., Mahmood, F., et al. (2018). Amphiregulin-producing gammadelta T cells are vital for safeguarding oral barrier immune homeostasis. Proc. Natl. Acad. Sci. USA *115*, 10738–10743. https://doi.org/10.1073/pnas.1802320115.
26. Wilharm, A., Tabib, Y., Nassar, M., Reinhardt, A., Mizraji, G., Sandrock, I., Heyman, O., Barros-Martins, J., Aizenbud, Y., Khalaileh, A., et al. (2019). Mutual interplay between IL-17-producing gammadeltaT cells and microbiota orchestrates oral mucosal homeostasis. Proc. Natl. Acad. Sci. USA *116*, 2652–2661. https://doi.org/10.1073/pnas.1818812116.
27. Van Dyken, S.J., Mohapatra, A., Nussbaum, J.C., Molofsky, A.B., Thornton, E.E., Ziegler, S.F., McKenzie, A.N.J., Krummel, M.F., Liang, H.E., and Locksley, R.M. (2014). Chitin activates parallel immune modules that direct distinct inflammatory responses via innate lymphoid type 2 and gammadelta T cells. Immunity *40*, 414–424. https://doi.org/10.1016/j.immuni.2014.02.003.
28. Sutherland, T.E., Logan, N., Rückerl, D., Humbles, A.A., Allan, S.M., Papayannopoulos, V., Stockinger, B., Maizels, R.M., and Allen, J.E. (2014). Chitinase-like proteins promote IL-17-mediated neutrophilia in a tradeoff between nematode killing and host damage. Nat. Immunol. *15*, 1116–1125. https://doi.org/10.1038/ni.3023.
29. Ajendra, J., Chenery, A.L., Parkinson, J.E., Chan, B.H.K., Pearson, S., Colombo, S.A.P., Boon, L., Grencis, R.K., Sutherland, T.E., and Allen, J.E. (2020). IL-17A both initiates, via IFNgamma suppression, and limits the pulmonary type-2 immune response to nematode infection. Mucosal Immunol. *13*, 958–968. https://doi.org/10.1038/s41385-020-0318-2.

30. Chen, F., Liu, Z., Wu, W., Rozo, C., Bowdridge, S., Millman, A., Van Rooijen, N., Urban, J.F., Jr., Wynn, T.A., and Gause, W.C. (2012). An essential role for TH2-type responses in limiting acute tissue damage during experimental helminth infection. Nat. Med. *18*, 260–266. https://doi.org/10.1038/nm.2628.

31. Walter, M.J., Kajiwara, N., Karanja, P., Castro, M., and Holtzman, M.J. (2001). Interleukin 12 p40 production by barrier epithelial cells during airway inflammation. J. Exp. Med. *193*, 339–351. https://doi.org/10.1084/jem.193.3.339.

32. Ohsaki, A., Venturelli, N., Buccigrosso, T.M., Osganian, S.K., Lee, J., Blumberg, R.S., and Oyoshi, M.K. (2018). Maternal IgG immune complexes induce food allergen-specific tolerance in offspring. J. Exp. Med. *215*, 91–113. https://doi.org/10.1084/jem.20171163.

33. Caruso, R., Ono, M., Bunker, M.E., Núñez, G., and Inohara, N. (2019). Dynamic and asymmetric changes of the microbial communities after cohousing in laboratory mice. Cell Rep. *27*, 3401–3412.e3. https://doi.org/10.1016/j.celrep.2019.05.042.

34. Papotto, P.H., Ribot, J.C., and Silva-Santos, B. (2017). IL-17(+) gammadelta T cells as kick-starters of inflammation. Nat. Immunol. *18*, 604–611. https://doi.org/10.1038/ni.3726.

35. Kumar, P., Monin, L., Castillo, P., Elsegeiny, W., Horne, W., Eddens, T., Vikram, A., Good, M., Schoenborn, A.A., Bibby, K., et al. (2016). Intestinal interleukin-17 receptor signaling mediates reciprocal control of the gut microbiota and autoimmune inflammation. Immunity *44*, 659–671. https://doi.org/10.1016/j.immuni.2016.02.007.

36. Zenewicz, L.A., Yin, X., Wang, G., Elinav, E., Hao, L., Zhao, L., and Flavell, R.A. (2013). IL-22 deficiency alters colonic microbiota to be transmissible and colitogenic. J. Immunol. *190*, 5306–5312. https://doi.org/10.4049/jimmunol.1300016.

37. Ahuja, M., Schwartz, D.M., Tandon, M., Son, A., Zeng, M., Swaim, W., Eckhaus, M., Hoffman, V., Cui, Y., Xiao, B., et al. (2017). Orai1-Mediated antimicrobial secretion from pancreatic acini shapes the gut microbiome and regulates gut innate immunity. Cell Metabol. *25*, 635–646. https://doi.org/10.1016/j.cmet.2017.02.007.

38. Langille, M.G.I., Zaneveld, J., Caporaso, J.G., McDonald, D., Knights, D., Reyes, J.A., Clemente, J.C., Burkepile, D.E., Vega Thurber, R.L., Knight, R., et al. (2013). Predictive functional profiling of microbial communities using 16S rRNA marker gene sequences. Nat. Biotechnol. *31*, 814–821. https://doi.org/10.1038/nbt.2676.

39. Zhang, L., Wu, W., Lee, Y.K., Xie, J., and Zhang, H. (2018). Spatial heterogeneity and Co-occurrence of mucosal and luminal microbiome across swine intestinal tract. Front. Microbiol. *9*, 48. https://doi.org/10.3389/fmicb.2018.00048.

40. He, Z., Ma, Y., Yang, S., Zhang, S., Liu, S., Xiao, J., Wang, Y., Wang, W., Yang, H., Li, S., and Cao, Z. (2022). Gut microbiota-derived ursodeoxycholic acid from neonatal dairy calves improves intestinal homeostasis and colitis to attenuate extended-spectrum beta-lactamase-producing enteroaggregative Escherichia coli infection. Microbiome *10*, 79. https://doi.org/10.1186/s40168-022-01269-0.

41. Thio, C.L.P., Chi, P.Y., Lai, A.C.Y., and Chang, Y.J. (2018). Regulation of type 2 innate lymphoid cell-dependent airway hyperreactivity by butyrate. J. Allergy Clin. Immunol. *142*, 1867–1883.e12. https://doi.org/10.1016/j.jaci.2018.02.032.

42. Selenko-Gebauer, N., Majdic, O., Szekeres, A., Höfler, G., Guthann, E., Korthäuer, U., Zlabinger, G., Steinberger, P., Pickl, W.F., Stockinger, H., et al. (2003). B7-H1 (programmed death-1 ligand) on dendritic cells is involved in the induction and maintenance of T cell anergy. J. Immunol. *170*, 3637–3644. https://doi.org/10.4049/jimmunol.170.7.3637.

43. Gundra, U.M., Girgis, N.M., Ruckerl, D., Jenkins, S., Ward, L.N., Kurtz, Z.D., Wiens, K.E., Tang, M.S., Basu-Roy, U., Mansukhani, A., et al. (2014). Alternatively activated macrophages derived from monocytes and tissue macrophages are phenotypically and functionally distinct. Blood *123*, e110–e122. https://doi.org/10.1182/blood-2013-08-520619.

44. Brodin, P., Jojic, V., Gao, T., Bhattacharya, S., Angel, C.J.L., Furman, D., Shen-Orr, S., Dekker, C.L., Swan, G.E., Butte, A.J., et al. (2015). Variation in the human immune system is largely driven by non-heritable influences. Cell *160*, 37–47. https://doi.org/10.1016/j.cell.2014.12.020.

45. Olszak, T., An, D., Zeissig, S., Vera, M.P., Richter, J., Franke, A., Glickman, J.N., Siebert, R., Baron, R.M., Kasper, D.L., and Blumberg, R.S. (2012). Microbial exposure during early life has persistent effects on natural killer T cell function. Science *336*, 489–493. https://doi.org/10.1126/science.1219328.

46. Moon, C., Baldridge, M.T., Wallace, M.A., Burnham, C.A.D., Stappenbeck, T.S., Virgin, H.W., and Stappenbeck, T.S. (2015). Vertically transmitted faecal IgA levels determine extra-chromosomal phenotypic variation. Nature *521*, 90–93. https://doi.org/10.1038/nature14139.

47. Robertson, S.J., Lemire, P., Maughan, H., Goethel, A., Turpin, W., Bedrani, L., Guttman, D.S., Croitoru, K., Girardin, S.E., and Philpott, D.J. (2019). Comparison of Co-housing and littermate methods for microbiota standardization in mouse models. Cell Rep. *27*, 1910–1919.e2. https://doi.org/10.1016/j.celrep.2019.04.023.

48. Ostaff, M.J., Stange, E.F., and Wehkamp, J. (2013). Antimicrobial peptides and gut microbiota in homeostasis and pathology. EMBO Mol. Med. *5*, 1465–1483. https://doi.org/10.1002/emmm.201201773.

49. Lahl, K., Sweere, J., Pan, J., and Butcher, E. (2014). Orphan chemoattractant receptor GPR15 mediates dendritic epidermal T-cell recruitment to the skin. Eur J Immunol. *44*, 2577–2581. https://doi.org/10.1002/eji.201444628.

50. Sezin, T., Jegodzinski, L., Meyne, L.M., Gupta, Y., Mousavi, S., Ludwig, R.J., Zillikens, D., and Sadik, C.D. (2021). The G protein-coupled receptor 15 (GPR15) regulates cutaneous immunology by maintaining dendritic epidermal T cells and regulating the skin microbiome. Eur. J. Immunol. *51*, 1390–1398. https://doi.org/10.1002/eji.202048887.

51. Ferretti, P., Pasolli, E., Tett, A., Asnicar, F., Gorfer, V., Fedi, S., Armanini, F., Truong, D.T., Manara, S., Zolfo, M., et al. (2018). Mother-to-Infant microbial transmission from different body sites shapes the developing infant gut microbiome. Cell Host Microbe *24*, 133–145.e5. https://doi.org/10.1016/j.chom.2018.06.005.

52. McCarthy, K.M., Gong, J.L., Telford, J.R., and Schneeberger, E.E. (1992). Ontogeny of Ia+ accessory cells in fetal and newborn rat lung. Am. J. Respir. Cell Mol. Biol. *6*, 349–356. https://doi.org/10.1165/ajrcmb/6.3.349.

53. Luu, M., Pautz, S., Kohl, V., Singh, R., Romero, R., Lucas, S., Hofmann, J., Raifer, H., Vachharajani, N., Carrascosa, L.C., et al. (2019). The short-chain fatty acid pentanoate suppresses autoimmunity by modulating the metabolic-epigenetic crosstalk in lymphocytes. Nat. Commun. *10*, 760. https://doi.org/10.1038/s41467-019-08711-2.

54. Luu, M., Riester, Z., Baldrich, A., Reichardt, N., Yuille, S., Busetti, A., Klein, M., Wempe, A., Leister, H., Raifer, H., et al. (2021). Microbial short-chain fatty acids modulate CD8(+) T cell responses and improve adoptive immunotherapy for cancer. Nat. Commun. *12*, 4077. https://doi.org/10.1038/s41467-021-24331-1.

55. Bäckhed, F., Roswall, J., Peng, Y., Feng, Q., Jia, H., Kovatcheva-Datchary, P., Li, Y., Xia, Y., Xie, H., Zhong, H., et al. (2015). Dynamics and stabilization of the human gut microbiome during the first year of life. Cell Host Microbe *17*, 852. https://doi.org/10.1016/j.chom.2015.05.012.

56. Rasmussen, M.A., Thorsen, J., Dominguez-Bello, M.G., Blaser, M.J., Mortensen, M.S., Brejnrod, A.D., Shah, S.A., Hjelmsø, M.H., Lehtimäki, J., Trivedi, U., et al. (2020). Ecological succession in the vaginal microbiota during pregnancy and birth. ISME J. *14*, 2325–2335. https://doi.org/10.1038/s41396-020-0686-3.

57. Yilmaz, B., Mooser, C., Keller, I., Li, H., Zimmermann, J., Bosshard, L., Fuhrer, T., Gomez de Agüero, M., Trigo, N.F., Tschanz-Lischer, H., et al. (2021). Long-term evolution and short-term adaptation of microbiota strains and sub-strains in mice. Cell Host Microbe *29*, 650–663.e9. https://doi.org/10.1016/j.chom.2021.02.001.

58. Lawrence, R.A., Gray, C.A., Osborne, J., and Maizels, R.M. (1996). Nippostrongylus brasiliensis: cytokine responses and nematode expulsion in normal and IL-4-deficient mice. Exp. Parasitol. *84*, 65–73. https://doi.org/10.1006/expr.1996.0090.

59. McDonald, D., Price, M.N., Goodrich, J., Nawrocki, E.P., DeSantis, T.Z., Probst, A., Andersen, G.L., Knight, R., and Hugenholtz, P. (2012). An improved Greengenes taxonomy with explicit ranks for ecological and evolutionary analyses of bacteria and archaea. ISME J. *6*, 610–618. https://doi.org/10.1038/ismej.2011.139.

60. Caporaso, J.G., Kuczynski, J., Stombaugh, J., Bittinger, K., Bushman, F.D., Costello, E.K., Fierer, N., Peña, A.G., Goodrich, J.K., Gordon, J.I., et al. (2010). QIIME allows analysis of high-throughput community sequencing data. Nat. Methods *7*, 335–336. https://doi.org/10.1038/nmeth.f.303.

61. Bolyen, E., Rideout, J.R., Dillon, M.R., Bokulich, N.A., Abnet, C.C., Al-Ghalith, G.A., Alexander, H., Alm, E.J., Arumugam, M., Asnicar, F., et al. (2019). Reproducible, interactive, scalable and extensible microbiome data science using QIIME 2. Nat. Biotechnol. *37*, 852–857. https://doi.org/10.1038/s41587-019-0209-9.

62. McMurdie, P.J., and Holmes, S. (2013). phyloseq: an R package for reproducible interactive analysis and graphics of microbiome census data. PLoS One *8*, e61217. https://doi.org/10.1371/journal.pone.0061217.

63. Yilmaz, B., Juillerat, P., Øyås, O., Ramon, C., Bravo, F.D., Franc, Y., Fournier, N., Michetti, P., Mueller, C., Geuking, M., et al. (2019). Microbial network disturbances in relapsing refractory Crohn's disease. Nat. Med. *25*, 323–336. https://doi.org/10.1038/s41591-018-0308-z.

64. Mallick, H., Rahnavard, A., McIver, L.J., Ma, S., Zhang, Y., Nguyen, L.H., Tickle, T.L., Weingart, G., Ren, B., Schwager, E.H., et al. (2021). Multivariable association discovery in population-scale meta-omics studies. Preprint at bioRxiv. https://doi.org/10.1101/2021.01.20.427420.

65. Douglas, G.M., Maffei, V.J., Zaneveld, J.R., Yurgel, S.N., Brown, J.R., Taylor, C.M., Huttenhower, C., and Langille, M.G.I. (2020). PICRUSt2 for prediction of metagenome functions. Nat. Biotechnol. *38*, 685–688. https://doi.org/10.1038/s41587-020-0548-6.

STAR★METHODS

KEY RESOURCES TABLE

REAGENT or RESOURCE	SOURCE	IDENTIFIER
Antibodies		
anti-CD3 (145.2C11)	BD Biosciences	AB_394591
anti-CD3 (17A2)	BioLegend	AB_1595492
anti-TCRδ (GL3)	BioLegend	AB_313832
anti-CD90.2 (Thy1.2; 53–2.1)	BioLegend	AB_2650924
anti-CD19 (6D5)	BioLegend	AB_313645
anti-CD23 (B3B4)	BioLegend	AB_312833
anti-CD45 (30F11)	BioLegend	AB_2563061
anti-CD4 (GK1.5)	BioLegend	AB_312693
anti-NK1.1 (PK136)	BioLegend	AB_313395
anti-PD-L1 (10F.9G2)	BioLegend	AB_2563619
anti-PD-L2 (TY25)	BioLegend	AB_2728123
anti-CD11b (M1/70)	BioLegend	AB_2562904
anti-ST2 (IL-33R; DIH9)	BioLegend	AB_2561917
anti-CD11c (N418)	BioLegend	AB_313777
anti-Sca-1 (D7)	BioLegend	AB_493596
anti-Gr-1 (RB6-8C5)	BioLegend	AB_313373
anti-Ly6G (1A8)	BioLegend	AB_1877261
anti-Ly6C (HK1.4)	BioLegend	AB_1732076
anti-IA/IE (MHC II; M5/114.15.2)	BioLegend	AB_2650896
anti-CD24 (M1/69)	BioLegend	AB_312839
anti-Siglec-F (E50-2440)	BD Biosciences	AB_2687570
anti-CD64 (X54-5/7.1)	BioLegend	AB_2629778
anti-CD206 (CO68C2)	BioLegend	AB_2561992
anti-IL-13 (eBio13A)	eBiosciences	AB_2573530
anti-IL-9 (RM9A4)	BioLegend	AB_2562730
IL-5 (TRFK5)	BioLegend	AB_315330
Chemicals, peptides, and recombinant proteins		
Sodium hexanoate, 99–100%	Sigma-Aldrich	10051-44-2
Sodium acetate, anhydrous, for molecular biology, ≥99%	Sigma-Aldrich	127-09-3
Sodium pentanoate	Fluorochem	6106-41-8
Sodium butyrate	Sigma-Aldrich	156-54-7
Recombinant Mouse IL-33 Protein	Biotechne	Cat#3626-ML-010/CF
Critical commercial assays		
LEGENDplex™ Mouse Cytokine Panel 2 (13-plex)	BioLegend	Cat#740134
LEGENDplex™ Mouse Immunoglobulin Isotyping Panel (6-plex) with V-bottom Plate	BioLegend	Cat#740493
LEGENDplex™ MU Th1/Th2 Panel (8-plex) w/VbP V02	BioLegend	Cat#741054
RNeasy Micro Kit	Qiagen	Cat#74004
QIAamp Fast DNA Stool Mini Kit	Qiagen	Cat#51604

(*Continued on next page*)

Continued

REAGENT or RESOURCE	SOURCE	IDENTIFIER
Deposited data		
Metagenomic Raw Sequencing Data	This paper	https://figshare.com/s/77865dbbf0daab588b8d
16S rRNA Amplicon Sequencing Data	This paper	https://figshare.com/s/77865dbbf0daab588b8d
Experimental models: Organisms/strains		
Mouse: B6: C57BL/6J	The Jackson Laboratory	IMSR_JAX:000664
Mouse: TCR$\delta^{-/-}$: B6.129P2-*Tcrd*^{tm1Mom}/J	The Jackson Laboratory	IMSR_JAX:002120
Mouse: JHT: B6.129P2-*Igh-J*^{tm1Cgn}/J	Instituto Gulbenkian de Ciências	IMSR_JAX:002438
Mouse: IL-17$^{-/-}$: B6.IL-17$^{-/-}$	Instituto de Medicina Molecular	MGI: 5695091
Mouse: IL-22$^{-/-}$: B6.IL-22$^{-/-}$	The University of Manchester	MGI: 4453827
Oligonucleotides		
qPCR primers	Sigma-Aldrich	See Table S1
Software and algorithms		
Graphpad Prism v9.0a	GraphPad Software, LLC	www.graphpad.com
FlowJo v10.1	Tree Star	https://www.flowjo.com
LEGENDplex™ Data Analysis Software Suite	Qognit	https://legendplex.qognit.com/user/login
QIIME v1.9.1	Caporaso et al., 2010	http://qiime.org
R (v3.6.2)	Packages for analytical parts: tidyverse, ape, vegan, nlme, stats, DEseq2, edgeR, ggtree	https://www.r-project.org/
phyloseq	Bolyen et al., 2019; McMurdie and Holmes, 2013	https://joey711.github.io/phyloseq/
PICRUSt2	Douglas et al., 2020	https://github.com/picrust/picrust2/releases
MaAsLin2	Morgan et al., 2012	https://huttenhower.sph.harvard.edu/maaslin/

RESOURCE AVAILABILITY

Lead contact

Further information and requests for resources and reagents should be directed to and will be fulfilled by the lead contact, Bruno Silva-Santos (bssantos@medicina.ulisboa.pt).

Materials availability

This study did not generate new unique reagents.

Data and code availability

- 16S rRNA amplicon sequencing dataset with processed files and the entire details of used samples can be downloaded using the following link: https://figshare.com/s/77865dbbf0daab588b8d (https://doi.org/10.6084/m9.figshare.15121245). Any additional information required to reanalyze the data reported in this paper is available from the co-author, Bahtiyar Yilmaz (bahtiyar.yilmaz@unibe.ch), upon request. This paper does not report original code.

EXPERIMENTAL MODEL AND SUBJECT DETAILS

Mice and breeding setups

C57BL/6J (B6) mice were purchased from Charles River Laboratories, C57BL/6J.TCR$\delta^{-/-}$ (referred to as TCR$\delta^{-/-}$, hereon in) were purchased from The Jackson Laboratory. C57BL/6J.JHT (referred as JHT) mice were obtained from Instituto Gulbenkian de Ciência (Oeiras, Portugal). All the mouse lines were bred and maintained in the specific pathogen-free animal facilities of Instituto de Medicina Molecular João Lobo Antunes (Lisbon, Portugal), with the exception of IL-22$^{-/-}$, which were generated and acquired from Jean-Cristophe Renauld, and bred in-house at The University of Manchester. After reaching sexual maturity (at around 8 weeks) TCR$\delta^{-/-}$ females were crossed with TCR$\delta^{+/-}$ males (obtained from the cross of TCRδ heterozygous animals derived, in turn, from a TCR$\delta^{-/-}$ x B6 breeding), and vice-versa; the pups obtained from the aforementioned crossings were kept with the parents until weaning, to be later divided by sex. All the pups were used at PN16 ± 2, unless stated otherwise.

Study approval

All experiments performed in Lisbon involving animals were done in compliance with the relevant laws and institutional guidelines and were approved by local and European ethic committees. All animal experiments were performed in Manchester are in accordance with the UK Animals (Scientific Procedures) Act of 1986 under a Project License (70/8548) granted by the UK Home Office and approved by the University of Manchester Animal Welfare and Ethical Review Body. Euthanasia was performed by asphyxiation in a rising concentration of carbon dioxide.

METHOD DETAILS

Cross-fostering and C-Sec surgeries

For cross-fostering experiments, mice were time-mated. Briefly, female mice were put in a cage containing the bedding of a cage containing male animals for a period of 48h. After this period of time, 1 or 2 females were introduced to a single-housed male. The following day, the presence of vaginal plugs (considered as E0.5) was recorded and males were transferred into a new cage. In some cases, the animals were left together for 2 days. Subsequently, pups born from a TCR$\delta^{-/-}$ dam were swapped with those from a TCR$\delta^{+/-}$ dam at day 1 post-birt (and vice-versa), respecting litter sizes (differences of 3 pups maximum).

For C-Sec experiments TCR$\delta^{+/-}$ and TCR$\delta^{-/-}$ females were bred with males from the opposing genotype in two groups, with an interval of 1 day between them. The group of females giving birth first was then defined as the surrogate mothers. Between days 18.5 and 19.5 the females from the second group underwent C-Sec surgery. Briefly, females are euthanized; the uterus is removed and submerged in iodine. Pups are taken out from the uterus on top of a sterile heated plate, cleaned and reanimated. When presenting regular respiratory movements, pups are put together with surrogate dams (from the same genotype of their own dam) and their progeny.

Cell preparation, flow cytometry, and analysis

For cell surface staining, single-cell suspensions were incubated in presence of anti-CD16/CD32 (eBioscience) with saturating concentrations of combinations of the mAbs listed above. Lungs were dissected and tissue was cut into pieces, then digested with collagenase D (0.66 mg/mL; Roche) and DNase I (0.10 mg/mL) (Sigma-Aldrich) in RPMI 1640 containing 5% Fetal Bovine Serum (FBS) at 37°C for 30 min. For lamina propria cell preparation, small intestines were dissected, washed in ice-cold PBS and Peyer's patches were excised. The organ was then cut into pieces and incubated with EDTA 0.05M at 37°C for 20 min; cells were then washed and passed through a 100-μm cell strainer and then digested as the lungs. Single cells were isolated by passing the tissue through a 40-μm cell strainer, followed by a 70%/20% Percoll (Sigma-Aldrich) gradient and 30-min centrifugation at 2400 rpm. Leukocytes were recovered from the interface, resuspended, and used for further analyses.

For intracellular cytokine staining, cells were stimulated with PMA (phorbol 12-myristate 13-acetate) (50 ng/mL) and ionomycin (1 μg/mL), in the presence of Brefeldin A (10 μg/mL) (all from Sigma) for 3h–4h at 37°C. Cells were stained for the identified above cell surface markers, fixed 30 min at 4°C and permeabilized with the Foxp3/Transcription Factor Staining Buffer set (eBioscience) in the presence of anti-CD16/CD32 (eBioscience) for 10 min at 4°C, and finally incubated for 1h at room temperature with identified above cytokine-specific Abs in permeabilization buffer. Cells were analyzed using FACSFortessa (BD Biosciences) and FlowJo software (Tree Star).

For cell sorting of lung interstitial macrophages (IM), lung cell suspensions were prepared and immuno-stained as described above. IM were defined as CD45$^+$CD64$^+$CD24$^-$CD11b$^+$CD11c$^-$ live cells, and then electronically sorted on a FACSAria (BD Biosciences) into sterile RNase-free eppendorfs containing 200μL of lysis buffer (Qiagen), for posterior mRNA isolation. For cell sorting of ILC2s, lung cell suspensions were prepared and immuno-stained as described above. ILC2s were defined as CD45$^+$Lin$^-$Thy1.2$^+$CD127$^+$ST2$^+$ live cells.

In-vitro ILC2 stimulation

To maximise cell yield for sort-purification, mice were injected intraperitoneally with 1μg of recombinant IL-33 (BioTechne) on day 0, 2, 4 and 6. Mice were culled on day 7, lungs were then processed and stained as described before for cell sorting.

Sorted ILC2s were plated at a density of 70,000 cells/well (round bottom plate) in 200uL of GlutaMAX media (Gibco) (supplemented with 10% FBS, 1% MEM Non-Essential Amino Acids Solution (100X) (Gibco), 1% Penicillin-Streptomycin (Sigma), 1% Sodium pyruvate solution 100mM (Sigma), and β-mercaptoethanol (Sigma)) with IL-7 (25 ng/mL, Peprotech). Cells were stimulated with IL-33 (20 ng/mL, BioTechne) plus the individual SCFA acetate (0.25mM), pentanoate (0.25mM), hexanoate (0.25mM) or Butyrate (0.25mM) or a cocktail containing the first three SCFA (acetate, 0.25mM; pentanoate, 0.125mM; hexanoate, 0.125mM). Cells were incubated for 24 h at 37°C in the presence of CO2, stained intracellularly for IL-13 and IL-5 and analyzed using FACSFortessa (BD Biosciences).

Immuno-detection of cytokines in lung tissue samples

Lung tissue was homogenized in 2 mL sterile tubes containing PBS plus a cocktail of protease inhibitors (cOmplete ULTRA tablets, Mini; Roche) and 1mm of diameter zirconia/silica beads (BioSpec Products), with the help of a tissue homogenizer. The homogenate was centrifuged in order to remove cellular debris and beads, and stored at −80°C until usage. Cytokine concentrations were assessed using LEGENDplex Mouse Th1/Th2 and Mouse Cytokine Panel 2 kits – both bead-based assays that use the principles of

sandwich ELISA to quantify soluble analytes using a flow cytometer (Biolegend) – according to manufacturer's instruction. Cytokine concentrations were normalized using total protein concentration in tissue homogenate, determined in a NanoDrop spectrophotometer (ThermoFisher).

Immuno-detection of antibodies in serum samples

Blood was collected from the cheek pouch in adults, and from decapitation in pups. Serum samples were then stored at −20°C until usage. Determination of immunoglobulins isotypes and serum concentrations were assessed using LEGENDplex Mouse Immunoglobulin Isotyping Panel (Biolegend) according to manufacturer's instruction.

RNA isolation, cDNA preparation and real-time PCR

mRNA was prepared from tissue homogenates using RNeasy Mini Kit (Qiagen). Reverse transcription was performed with random oligonucleotides (Invitrogen) using Moloney murine leukemia virus reverse transcriptase (Promega) for 1 h at 42°C. Relative quantification of specific cDNA species to endogenous reference *Hprt*, *Actb* or *β2microglobulin* was carried out using SYBR on ABI ViiA7 cycler (Applied Biosystems). The C_T for the target gene was subtracted from the average C_T for endogenous references, and the relative amount was calculated as $2^{-\Delta CT}$.

N. brasiliensis *infection*

N. brasiliensis was maintained by serial passage through Sprague-Dawley rats, as previously described.[58] Third-stage larvae (L3) were washed ten times with sterile PBS prior to subcutaneous infection of 300 L3s per mouse. On day 6 post-infection (p.i.) lungs were excised and processed accordingly to the analysis to be conducted.

Histology and histopathological analysis

Lung samples were fixed in 10% neutral buffered formalin and processed for paraffin embedding, sectioned and stained with Hematoxylin-Eosin. Each slide was digitalized using a NanoZoomer-SQ Digital slide scanner. To quantify emphysema like damage, we used the Linear Mean Intercepts (LMI) method. After digitalization of each lung slide, between 10 and 20 non-overlapping pictures, of each lung, were taken. The pictures were analyzed using ImageJ software. For each picture, 6 horizontal lines were drawn. For the LMI calculation, the length of the line was multiplied by the number of pictures taken and the number of lines in one picture, and then divided by the total number of times a line intercepted an alveolus.

Antibiotic treatment and SCFA supplementation

$TCR\delta^{-/-}$ and $TCR\delta^{+/-}$ female and male adult mice were maintained with a mixture of antibiotics (5 mg/mL of streptomycin, 1 mg/mL of ampicilin, 1 mg/mL of collistin, and 0.5 mg/mL of vancomycin; Sigma Aldrich) in the drinking water for at least three weeks prior the start of the breedings, and then crossed as already described. Antibiotic treatment was kept for the whole duration of pregnancy and fostering.

For direct supplementation of SCFA, 50μL of a cocktail containing acetate (2 mg/mL), pentanoate (0.4 mg/mL) and hexanoate (0.35 mg/mL) was administered i.p. 3 times/week, starting at PN7 and finishing at PN13 for experiments analyzing the steady-state lung; and starting at PN14 and finishing at PN20 for experiments analyzing the response to *N. brasiliensis* infection. In both cases controls were injected with PBS. When given to dams, an SCFA cocktail containing acetate (50mM), pentanoate (37.5mM) and hexanoate (12.5mM) was added to the drinking water at day 2 ± 1 after the litter was born and kept during the fostering period.

Microbiota profiling via 16S rRNA gene sequencing

Samples were collected in sterilized surfaces using autoclaved materials. Fecal microbiota was assessed from two to three fecal pellets per animal. Skin microbiota was assessed upon removal of one ear per animal. Vaginal microbiota was assessed from the vaginal wash with 30μL of sterile PBS. Lung and cecum mucosa associated microbiota were assessed from the whole excised organs. Immediately after collection, samples were snap-frozen in liquid nitrogen and stored at −80°C until microbial DNA extraction. Before extraction, samples were homogenized in 2mL sterile tubes containing 1mm of diameter autoclaved zirconia/silica beads (BioSpec Products), with the help of tissue homogenizer. Microbial genomic DNA was extracted using the QIAamp Fast DNA Stool Mini kit (Qiagen). The 16S rRNA V4 amplicons and ITS1-spanning amplicons were both generated using the following Earth Microbiome Project benchmarked protocols. Amplicons were then sequenced using on a 2 × 250bp PE mode Illumina MiSeq platform at Instituto Gulbenkian de Ciências (IGC) Genomics Unit (Oeiras, Portugal).

Raw sequences obtained from 2 independent Illumina MiSeq runs were initially pooled and analyzed in the QIIME pipeline version 2 using custom analysis scripts for analysis on the UBELIX Linux cluster of the University of Bern (High-Performance Computing, University of Bern, Bern, Switzerland). Amplicon sequencing variants were assigned using Greengenes (13_8) databases with the *feature-classifier classify-sklearn* function for 97% sequence identity threshold.[59] The taxonomy, rep-seqs, and rooted-tree files generated in QIIME2 were called out in the phyloseq pipeline in R. Calculation and plotting of the alpha diversity (Simpson and Shannon index), beta diversity (Bray-Curtis dissimilarities on NMDS plot), and statistical analysis using Adonis test were performed using phyloseq pipeline.[60–63] The multivariate analysis by linear models (MaAsLin2) was used to find associations between metadata and microbial community abundance (https://huttenhower.sph.harvard.edu/maaslin/).[64] Taxa that were present in ≥30% of the samples

and had >0.001% of total abundance were set as the cut-off values for further analysis. After Benjamini-Hochberg's false discovery rate correction, the adjusted p value (<0.05 or <0.2) was considered significant.

The prediction of metagenome functional content was performed using 16S sequencing data in the Phylogenetic Investigation of Communities by Reconstruction of Unobserved States (PICRUSt2) pipeline.[65] PICRUSt2 predictions were categorized as levels 1–3 and further into Kyoto Encyclopedia of Genes and Genomes pathways.

SCFA measurement

Sample analysis was carried out by MS-Omics (www.msomics.com) as follows. Samples extracted by adding ultrapure water to the cecum (100μL to samples with less than 30mg and 150μL to samples with more). The filtered cecum water was further extracted by addition of deuterium labeled internal standards and mixing with MTBE directly in the injection vial. All samples were analyzed in a randomized order. Analysis was performed using a high polarity column (ZebronTM ZB-FFAP, GC Cap. Column 30 m × 0.25 mm x 0.25μm) installed in a GC (7890B, Agilent) coupled with a quadropole detector (5977B, Agilent). The system was controlled by ChemStation (Agilent). Raw data was converted to netCDF format using Chemstation (Agilent), before the data was imported and processed. The raw GC-MS data was processed by software developed by MS-Omics and collaborators. The software uses the powerful PARAFAC2 model and can extract more compounds and cleaner MS spectra than most other GC-MS software.

Literature review

A search was performed in the PubMed database in May/2019, using the keywords "gamma delta T cells AND infection" and "gamma-delta T cells AND infection". Studies employing TCR$\delta^{-/-}$ mice were then divided regarding the use of littermates or genetic background-matched mice as controls. Journals were divided by their impact factor at the moment of the literature search.

QUANTIFICATION AND STATISTICAL ANALYSIS

Statistical analysis

In most experiments 3 independent litters were pooled together, unless stated otherwise. D'Agostino-Pearson normality test was applied to assess the normality of the populations analyzed; statistical significance of differences between populations was, then, assessed with the Student's t-test or by using a two-tailed nonparametric Mann-Whitney U test, when applicable. For grouped statistical analysis, two-Way ANOVA was employed. The p values < 0.05 were considered significant and are indicated on the figures.